The Effect of Crack Depth on Elastic-Plastic Fracture Toughness in Bend-Bar Specimens

By

William A. Sorem
Robert H. Dodds, Jr.
Stanley T. Rolfe

A Report on Research Sponsored by the

Pressure Vessel Research Committee of the Welding Research Council
American Iron and Steel Institute
David Taylor Research Center

Structural Engineering and Engineering Materials
SL Report 89-1
October, 1989

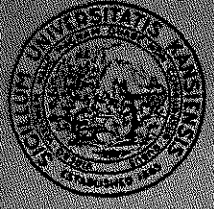

THE UNIVERSITY OF KANSAS CENTER FOR RESEARCH, INC.
2291 Irving Hill Drive--Campus West, Lawrence, Kansas 66045

EFFECTS OF CRACK DEPTH ON ELASTIC-PLASTIC FRACTURE TOUGHNESS IN BEND-BAR SPECIMENS

By

William A. Sorem
Exxon Production Research

Robert H. Dodds, Jr.
University of Illinois

Stanley T. Rolfe
University of Kansas

A Report on a Research Project Sponsored by the:

Pressure Vessel Research Committee of The Welding Research Council
American Iron And Steel Institute
David Taylor Research Center

OCTOBER 1989

ABSTRACT

Short crack test specimens ($a/W << 0.50$) are frequently employed when conventional deep crack specimens are either inappropriate or impossible to obtain, for example, in testing of particular microstructures in weldments and in-service structures containing shallow surface flaws. Values of elastic-plastic fracture toughness, here characterized by the crack tip opening displacement (CTOD), are presented for square (cross-section) three-point bend specimens with a/W ratios of 0.15 and 0.50 throughout the lower-shelf and lower-transition regions. Three-dimensional, finite-element analyses are employed to correlate the measured load and crack mouth opening displacement (CMOD) values to the corresponding CTOD values, thus eliminating a major source of experimental difficulty in previous studies of shallow crack specimens. In the lower-transition region, where extensive plasticity (but no ductile crack growth) precedes brittle fracture, critical CTOD values for short crack specimens are significantly larger (factor of 2-3) than the CTOD values for deep crack specimens at identical temperatures. Short crack specimens are shown to exhibit increased toughness at the initiation of ductile tearing and decreased brittle-to-ductile transition temperatures. Numerical analyses for the two a/W ratios reveal large differences in stress fields ahead of the crack tip at identical CTOD levels which verify the experimentally observed differences in critical CTOD values. Correlations of the predicted stresses with measured critical CTOD values demonstrate the limitations of single-parameter fracture mechanics (as currently developed) to characterize the response.

EFFECTS OF CRACK DEPTH ON ELASTIC-PLASTIC FRACTURE TOUGHNESS IN BEND-BAR SPECIMENS

1. Introduction

Laboratory testing of three-point-bend specimens to measure elastic-plastic fracture toughness, characterized here by the crack tip opening displacement (CTOD), generally focuses on one of three objectives: (1) to rank, or order, potential construction materials according to fracture resistance, (2) to provide fracture toughness values for failure or fitness-for-purpose studies, or (3) to insure a level of quality during construction, e.g., the fracture resistance of specific welding procedures. For the first objective, deeply cracked specimens are employed extensively; such specimens provide the most severe crack-tip conditions with resulting fracture toughness values that are invariant of the crack depth over the range $0.4 < a/W < 0.8$. No direct link with the crack-tip conditions in a flawed structural component is required for such material characterization studies. Unlike the first objective, the second objective of laboratory testing attempts to correlate directly the crack-tip conditions in the flawed structural component with those of the test specimen. In such cases, it frequently becomes necessary to employ short cracks ($a/W << 0.50$) in the test specimen to match more realistically the crack-tip conditions of the structural component containing, for example, a shallow surface flaw. The use of lower-bound toughness values from deeply notched specimens for this purpose may be unacceptable (overly conservative). Finally, for the third objective of laboratory testing, crack depths over the complete range of a/W ratios are required to assess the fracture toughness of various microstructures present in weldments; the fabrication of a deeply notched specimen with the crack tip sited in the microstructure of interest may not be physically possible -- the use of short crack specimens becomes the only practical alternative.

To correlate measured toughness values for short crack specimens with structural behavior, the effects of crack-depth to specimen-width ratio (a/W) on the behavior of the test specimen must first be understood. Moreover, an accurate procedure to obtain the toughness parameter from measurable quantities, load and crack mouth opening displacements (CMOD), is required over the complete range of a/W ratios. Recent investigators [1-10] have studied the effect of a/W ratio on measured fracture toughness values. Using slip-line theory, Matsoukas [1] suggests that a distinction between short and deep crack behavior occurs at a/W of 0.177, i.e., for a/W ratios less than 0.177 the plastic zone at the crack tip extends "backward" to the free (tension) surface prior to the development of a plastic hinge. But, because slip-line theory employs a rigid-perfectly plastic material, collapse occurs at the instant a plastic hinge develops in the specimen; consequently specimens with a/W ratios greater than 0.177 never yield to the free surface in a slip-line analysis. Materials with significant strain hardening may develop yielding to the tension surface for larger a/W ratios.

Experimental investigations have been conducted on short crack specimens (a/W = 0.15 to 0.20) using the CTOD test method [2–9]. The critical CTOD values at brittle fracture for the short crack specimens are reported to be 2–3 times the value for the deep crack specimens (a/W = 0.50). CTOD values at initiation of ductile tearing for short crack specimens are also reported to exceed values for deep crack specimens. Moreover, the transition from brittle–to–ductile crack initiation occurs at a lower temperature for the short crack specimens. Because these studies revealed such significant differences in fracture toughness for small and large a/W ratios, the current draft of the ASTM standard for CTOD testing restricts a/W ratios to 0.45–0.55 until a thorough understanding of the short crack behavior is developed.

In this investigation, laboratory tests and numerical analyses were performed to assess further the effects of crack–depth to specimen–width ratio (a/W) on fracture toughness, as measured in three–point bend CTOD specimens. Testing was conducted on an A36 steel using square cross–section, three–point bend specimens of dimensions 31.8 * 31.8 * 127 mm (1.25 * 1.25 * 5.0 in.) with a/W ratios of 0.15. Slow–bend tests were conducted at temperatures over the range of -195°C (-320°F) to 21°C (70°F). Results of the short crack (a/W = 0.15) CTOD specimens are compared to the results of the deep crack (a/W = 0.50) CTOD specimens, taken from the same A36 steel plate, tested previously by Sorem et al. [11].

Three–dimensional, finite–element analyses of the test specimens were employed to correlate the experimentally measured load and CMOD values to the corresponding CTOD values. This represents a significant improvement over earlier experimental studies of short crack specimens in which difficulties and uncertainties were encountered in inferring CTOD values from easily measured quantities (load, CMOD). The finite–element analyses are sufficiently detailed to allow comparisons of plastic deformation and stresses ahead of the crack tip for the two a/W ratios. Correlations of the predicted stresses with measured critical CTOD values (prior to stable crack growth) are used to examine the limitations of single–parameter fracture mechanics (as currently developed) to characterize the response.

The present study has three objectives. The first is to examine the effect of the a/W ratio on critical CTOD values throughout the lower shelf and lower transition regions in which fracture occurs prior to stable crack growth. A statistical evaluation of both mean and lower bound CTOD values is included. The second objective is to assess effects of the a/W ratio on CTOD values at the initiation of fibrous tearing. The third objective is to examine effects of the a/W ratio on the brittle–to–ductile transition temperature and the effects on scatter of CTOD values in this region.

2. Material Properties

A 31.8 mm (1.25 in.) thick, as–rolled plate of A36 steel was used in this study. Tables 1 and 2 provide the chemical analysis and mechanical properties of the steel. Table 3 also provides the yield strength of the A36 plate at various temperatures as determined by Shoe-

maker and Seeley [12]. Figure 1 shows the engineering stress–strain curve obtained from a standard 12.8 mm (0.505 in.) diameter longitudinal tensile test conducted at room temperature and a slow loading rate. At room temperature, the ultimate stress to yield stress ratio is 1.86 and the strain hardening exponent (n) is 0.23.

Charpy–V–Notch impact specimens from this plate (L–T orientation) were tested at temperatures ranging from –74°C (–100°F) to 82°C (180°F). The absorbed energy vs. temperature results are provided in Figure 2. The 20.4 J (15 ft. lbs.) absorbed energy transition occurs at approximately 4°C (40°F) and the 50 percent shear fracture appearance occurs at approximately 24°C (75°F). The upper shelf region develops at approximately 49°C (120°F) at which the notch toughness is approximately 136 J (100 ft. lbs.).

3. Testing Procedures

Square (B * B) three–point bend specimens with an a/W ratio of 0.15 were machined from the A36 steel plate. Specimens were prepared with crack planes oriented perpendicular to the rolling direction of the plate (L–T orientation). Because of the difficulty in obtaining straight fatigue cracks in short crack specimens, over–sized specimens with dimensions 31.8 * 54.6 * 127 mm (1.25 * 2.15 * 5.0 in.) were used with deep chevron notches to promote fatigue crack growth and straight fatigue cracks. Following fatigue pre–cracking, the specimens were re–machined to the square cross–section having dimensions 31.8 * 31.8 * 127 mm (1.25 * 1.25 * 5.0 in.) with an a/W ratio of 0.15 as shown in Figure 3. The resultant fatigue cracks satisfied the straightness requirements of the ASTM and British Standards specifications and very closely approximated the straight cracks modeled in the finite–element analysis. Figure 3 also illustrates the corresponding deep crack specimen with a/W = 0.50.

A 200 kN universal closed–loop testing machine was used for both fatigue cracking and the final ramp load failure. Crack mouth opening displacement (CMOD) was measured by a clip–gage mounted on knife edges machined into the specimen. Testing was conducted at temperatures ranging from –195°C (–320°F) to 21°C (70°F). Low temperatures were attained by submersion of the specimen in a heat transfer bath mounted on the test machine actuator. The specimens were held at the testing temperature for approximately 20 minutes and tested without removing them from the cooling bath.

4. Finite–Element Analysis Procedure

Figure 4 shows the 3–D analysis models constructed with 20–node isoparametric elements. Symmetry of the loading and constraints permit the use of one–quarter models of the specimens as shown in this figure. Elements incident on the crack front are degenerated into triangular prisms with the coincident nodes free to displace independently. This modeling procedure provides a $1/r$ strain singularity at points along the crack front corresponding to element corner nodes.

The finite–element models for the two specimens were constructed to facilitate comparisons of opening mode stresses on the crack plane. The first four rings of elements enclosing the crack tip were the same size in each model. Stresses in the two specimens were compared at the same absolute location from the crack tip [$r = 0.036$ mm (0.0142 in.)]. This location corresponded to the Gauss point nearest the crack plane and crack tip but outside the degenerated elements.

The use of degenerated, 20–node elements along the crack front provides a convenient means to extract CTOD values from computed displacements of the initially coincident nodes. The CTOD is defined as the separation of the crack flanks at the location where two rays drawn at right angles intercept the crack flanks. Figure 5 illustrates the initial and deformed crack–tip region and the definition of CTOD using the 90° intercept method.

Reduced integration (2 x 2 x 2) was used for all elements except those incident on the crack front. Full integration (3 x 3 x 3) of the crack–front elements was necessary to prevent physically unreasonable displacements arising from zero–energy modes. Plasticity was modelled using incremental theory with a von Mises yield surface, associated flow rule, and isotropic hardening. Conventional, linear strain–displacement relations were employed in the computations.

Material properties were taken from the engineering stress–strain curve shown in Figure 1. A piecewise linear approximation for this curve was used in the analyses. To improve numerical convergence, the yield plateau was replaced with a straight line from the yield point to a point of tangency on the strain hardening curve to produce a stress–strain curve with monotonically decreasing slope.

The finite–element models were loaded through displacements imposed on a line of nodes along the bottom of the uncracked ligament. As the size of the plastic zone increased, proportional displacements were imposed on the adjacent nodes to maintain consistency with observed local deformations caused by the loading roller.

The numerical computations were performed with the POLO–FINITE software [13,14].

5. Techniques to Interpret Experimental Results

5.1 *Temperature–toughness relation*

The temperature vs. fracture toughness relation for low–strength structural steels may be described by four regions as shown in Figure 6. These regions are designated: lower shelf, lower transition, upper transition, and upper shelf. The crack tip opening displacement test is currently the only fracture mechanics test method applicable (allowed by a testing "standard") in all four regions.

Linear–elastic fracture mechanics fully describes the behavior in the lower shelf region. In this region, limits on plastic deformation imposed in the ASTM E–399 and the

BS5447 test procedures are satisfied. The CTOD test thus yields valid measures of K_{Ic}. The load–CMOD relation remains linear to the point of failure and the fracture surface exhibits completely brittle behavior. CTOD results are designated as δ_c values in the lower shelf region.

The lower transition region requires characterization by elastic–plastic fracture mechanics. The load–CMOD relation at failure is no longer linear; plasticity at the crack tip is too extensive for application of linear–elastic fracture mechanics. A plastic hinge often develops prior to failure in the lower transition region. No stable crack growth is visible on the fracture surface and failure occurs by brittle fracture. CTOD results are reported as δ_c values in the lower transition region.

In the upper transition region stable crack growth occurs followed by brittle fracture. The load–CMOD record reflects extensive plastic deformation over the remaining ligament. Although ductile tearing is apparent on the fracture surface, final failure occurs by brittle fracture. The point at which fibrous tearing initiates ($\Delta a > 0$) often is determined with the use of crack growth resistance curves. CTOD results in the upper transition region are reported as δ_i values for initiation of fibrous tearing and as δ_u values for brittle fracture.

Fibrous initiation and extensive stable crack growth characterize the upper shelf region. The entire fracture surface is often fibrous and no crack growth instability is experienced. The load–CMOD record indicates extensive plastic deformation in the specimen. After reaching a peak load, additional displacements imposed at the load point lead to a gradual reduction in the supported load while stable crack growth continues. CTOD results in the upper shelf region are reported as δ_i values for initiation of fibrous tearing and as δ_m values at maximum load.

5.2 CTOD–CMOD Relation

The CTOD values are obtained from the measured load–CMOD records and the relation:

$$\delta = \frac{K^2(1-\nu^2)}{2\sigma_{ys}E} + \frac{RF(W-a)V_p}{RF(W-a)+a} \tag{1}$$

where K = theoretical stress intensity factor $= \dfrac{YP}{B\sqrt{W}}$

Y = stress intensity coefficient for a three–point bend specimen having span (S) = 4W:

$$= \frac{6(a/W)^{1/2}(1.99 - a/W[1-a/W][2.15 - 3.93(a/W) + 2.7(a/W)^2])}{(1+2a/W)(1-a/W)^{3/2}}$$

P = applied force

B = specimen thickness

W = specimen depth

ν = Poisson's ratio

σ_{ys} = 0.2% offset yield strength at temperature of interest
E = Young's modulus at temperature of interest
a = effective crack length (initial length + stable crack growth)
V_p = plastic component of clip-gage displacement
RF = plastic rotation factor

The first term of Eq. (1) provides the small-scale yielding (SSY) contribution which often is referred to as the elastic contribution. The second term provides the plastic contribution from large-scale yielding; it is based on the assumed rigid rotation of the specimen ends about a point on the crack plane ahead of the crack tip.

For deep crack specimens, the plastic rotation factor has been shown to lie between 0.40 and 0.46 by various investigators [15,16]. Strain hardening has a negligible effect on the rotation factor of deep crack specimens. The BS5762 form of Eq. (1) adopts a constant rotation factor of 0.40 which yields a conservative (lower) estimate of the critical CTOD.

The plastic rotation factor for short crack specimens depends on the crack-depth to specimen-width ratio (a/W) and on the strain hardening. Rotation factors have been determined experimentally using crack infiltration techniques [1,4,5,7] and also dual clip-gage techniques [4,6]. Depending on the experimental technique and the material properties, these studies have found rotation factors that vary between 0.20 and 0.45 for a/W = 0.15. For the A36 specimens tested in this study, the *3-D* finite-element analyses are used to determine the applicable rotation factors. Two independent procedures to obtain plastic rotation factors are considered. First, the linear-elastic displacement of the outer (traction-free) flanks of the crack profile are subtracted from the total displacement to determine the opening profile of the crack due only to plastic deformation in the specimen. Linear regression applied to the plastic displacements of the outer flanks of the crack profile provides the location of the plastic rotation point. In the second method, the finite-element load-CMOD response is treated as the experimental record. The CTOD value is taken directly from the deformed finite-element mesh using the 90° intercept technique. Consequently, the only unknown term in Eq. (1) becomes the plastic rotation factor (RF).

Figure 7 compares the CTOD taken from the deformed finite-element mesh and the CTOD computed from the finite-element load-CMOD record. Use of a plastic rotation factor of 0.4 (deep crack RF) in Eq. (1) considerably overestimates the large-scale yielding contribution of CTOD and therefore over estimates the total CTOD. A plastic rotation factor of 0.2 provides CTOD values in very close agreement with the CTOD taken directly from the deformed finite-element mesh.

5.3 Alternative Computation of Plastic CTOD

For small a/W ratios, the large-scale yielding component of CTOD, denoted δ_p, is defined from Eq. (1) as

$$\delta_p = \left(\frac{RF(W-a)}{RF(W-a)+a} \right) V_p \qquad (2)$$

δ_p is particularly sensitive to values employed for the rotation factor. This equation derives from the use of similar triangles to linearly relate the plastic CTOD to the plastic component of CMOD (V_p). As a/W ratios decrease, the distance from the crack tip to the rotation point, RF(W–a), becomes significantly larger than the crack depth (a). Consequently, a minor variation of the plastic CTOD–CMOD relationship causes a large fluctuation in RF. Dodds [17] suggests an alternate expression where the similar triangles derivation is replaced with a non-dimensional *eta* factor, η_δ, such that

$$\eta_\delta = \frac{\delta_p}{V_p} = \frac{RF(W-a)}{RF(W-a)+a} \tag{3}$$

η_δ is computed by applying linear regression to the plastic CTOD and CMOD values taken from the finite–element results. This approach appears to better reflect the actual sensitivity of the plastic CTOD–CMOD relationship. The total CTOD may thus be expressed in the form

$$\delta = \frac{K^2(1-\nu^2)}{2\ \sigma_{ys}\ E} + \eta_\delta\ V_p \tag{4}$$

The finite–element results indicate, using Eq.(1), RF = 0.20 for the A36 steel specimens with a/W = 0.15. Substitution of RF = 0.20 into Eq. (3) provides an η_δ factor of 0.53. The η_δ factor calculated directly from linear regression of the computed $\delta_p - V_p$ relationship is 0.51. Thus, in deriving experimental CTOD values from the experimental load–CMOD record, the use of Eq.(1) with RF = 0.20 and Eq.(4) with $\eta_\delta = 0.50$ yields identical CTOD values.

6. Experimental Results

6.1 Critical CTOD Values

Figure 8 presents critical CTOD values in the lower shelf and lower transition regions, –195°C (–320°F) to 21°C (70°F), for the short crack specimens. The temperature range over which valid K_{Ic} results are obtained defines the lower shelf. To meet the ASTM E–399 requirements for valid K_{Ic} results, the crack length, a, must be greater than a specified multiple of the plastic zone size

$$a > 2.5 \left(\frac{K_{Ic}}{\sigma_{ys}}\right)^2 \tag{5}$$

For a given material, short crack specimens must have lower K_{Ic} values to meet the E–399 requirements. Equation (5) was originally developed for testing in the a/W = 0.50 range and appears to be unduly restrictive for small a/W ratios. Only one of three short crack specimens tested at –195°C (–320°F) satisfied the initial crack length requirements of Eq.(5). Consequently, the lower shelf region is restricted to temperatures below –195°C (–320°F).

In the lower transition region, at temperatures between –107°C (–160°F) and –43°C (–45°F), specimens exhibit completely brittle behavior. Only one of the nine specimens

tested at –43°C (–45°F) experienced ductile tearing. The crack extension (Δa) of approximately 0.051 mm (2.0 mils) corresponds to a CTOD value at failure, δ_u, of 0.335 mm (13.2 mils). Note that these two quantities, namely crack growth and CTOD, both have units of length but are two separate measurements. Crack growth occurs in the fracture plane; CTOD is the opening displacement perpendicular to the two fracture surfaces. Thus, the two measurements are totally different although, in general, a larger crack growth (Δa) prior to failure would result in a larger CTOD (δ_u).

Specimens tested at –18°C (0°F) and 0°C (32°F) define the beginning of the upper transition region; they developed ductile thumbnails prior to brittle fracture. The results varied from approximately 0.051 mm (2.0 mils) of crack growth at a critical CTOD of 0.30 mm (12.0 mils) to approximately 0.76 mm (30 mils) of crack growth at a CTOD of 0.78 mm (30.8 mils). At 21°C (70°F), two specimens experienced significant crack growth before failing by brittle fracture. To determine the CTOD at initiation of ductile tearing, δ_i, the remaining specimens tested at 21°C (70°F) were unloaded at various displacement levels, i.e., corresponding to varying amounts of crack growth, and reloaded to failure after cooling to a temperature that ensured brittle fracture. Additional discussion of δ_i values is presented in the following section.

Figure 9 provides critical CTOD values for the deep crack (a/W = 0.50) specimens previously tested by Sorem et. al. [11]. The three specimens tested at –195°C (–320°F) are in the lower shelf region (valid K_{Ic}). The lower transition region extends from the lower shelf to the initiation of ductile tearing at test temperatures of approximately 0°C (32°F). At this temperature, the size of the ductile thumbnails ranged from 0.025 to 0.20 mm (1 to 8 mils) in depth. The boundary between brittle fracture (lower transition) and ductile tearing followed by brittle fracture (upper transition) occurs at a CTOD of approximately 0.2 mm (8 mils). Specimens tested at 21°C (70°F) experienced ductile thumbnails between 0.20 and 0.41 mm (8 and 16 mils) in depth before failing by brittle fracture.

Figure 10 compares critical CTOD values for the short and deep crack specimens. The solid line indicates lower bound values for the deep crack; it is constructed using the lowest test values obtained at each temperature. The dashed line shown in Figure 10 indicates the deep crack lower bound CTOD values multiplied by 2.5. This line very closely estimates the lowest experimental values obtained for the short crack specimens in the lower transition region. At –18°C (0°F) and 0°C (32°F), where limited ductile tearing precedes brittle fracture, the δ_u values are also approximately 2.5 times the deep crack CTOD (δ_c) results at the same temperature. At –195°C (–320°F) the CTOD values are essentially the same, although even at this temperature, the CTOD values of the short crack specimen are 20–30 percent higher than those of the deep crack specimen. However, the values are so small that for all practical purposes, there is no definitive effect of crack depth.

6.2 Ductile Initiation

The a/W ratio also affects the temperature and CTOD levels for the brittle–to–ductile transition, as defined by the first onset of ductile tearing prior to failure. The short crack specimen first develops a ductile thumbnail at –43°C (–45°F) with a CTOD level of ap-

proximately 0.30 mm (12 mils). The deep crack specimen first develops a ductile thumbnail at a temperature of 0°C (32°F) with a CTOD level of approximately 0.20 mm (8 mils). The CTOD value at transition is approximately 1.5 times greater for the short crack specimens than for the deep crack specimens; the transition temperature (as defined above) for the short crack specimens is considerably lower than the transition temperature for the deep crack specimens. These observations are based on the first appearance of a ductile thumbnail on the fracture surface which corresponds to 0.025 to 0.075 mm (1 to 3 mils) of crack extension.

Apparent crack extension caused by crack-tip blunting prior to actual, stable crack extension must be removed in the process of determining δ_i or J_{Ic} for both the CTOD and J-integral test procedures. A blunting line is constructed on the assumption that "apparent" crack extension due to crack-tip blunting equals one-half of the CTOD. Rather than constructing a blunting line, it has been proposed to use the CTOD value at the initiation of ductile tearing defined when the physical crack extension (Δa) reaches 0.20 mm (7.9 mils). The CTOD value for this amount of crack extension obviously is larger than the CTOD value at the first appearance of a ductile thumbnail and reflects efforts of the ASTM committee on CTOD testing to establish a definable quantity.

The initiation of ductile tearing for the short crack specimen was determined using the multi-specimen, R-curve technique at the 21°C (70°F) test temperature. Two specimens were tested to failure; each specimen exhibited slow stable crack growth followed by brittle fracture. The four remaining specimens were tested and unloaded at differing displacement levels to generate various amounts of crack extension. The specimens were then reloaded to failure after cooling to a temperature on the lower shelf to cause failure by cleavage. The crack extension (Δa) was measured and plotted vs. CTOD as shown in Figure 11. The CTOD at the onset of slow stable crack extension is the value at the intersection of the regression line and the $\Delta a = 0.20$mm (7.9 mils) offset line. Using this definition, ductile initiation for 21°C (70°F) occurs at a CTOD value of 0.46 mm (18.2 mils). The actual onset of ductile tearing, i.e., first visible tearing on the fracture surfaces, occurs at a CTOD value of about 0.30 mm (12 mils).

The initiation of ductile tearing for the short crack specimens was also determined at -18°C (0°F). Six specimens were tested to failure and exhibited varying amounts of slow stable crack growth before fracturing in a brittle manner. The measured crack extension vs. CTOD is shown in Figure 12. None of the data points exhibited more than 0.50 mm (20 mils) of crack extension, therefore δ_i was estimated as the minimum CTOD value of the three tests between the 0.15 mm (6.0 mils) and the 0.50 mm (20 mils) offset lines. Ductile initiation at -18°C (0°F) occurs at a CTOD value of 0.46 mm (18.2 mils). This value closely approximates the linear regression estimate of the CTOD data and also matches the initiation of ductile tearing at 21°C (70°F). No clear effect of temperature on δ_i values for the short crack specimen was found at -18 and 21°C (0° and 70°F).

Fracture surfaces of the deep crack specimens were examined to measure crack extension for specimens which revealed a ductile thumbnail. Three specimens were tested at

21°C (70°F) and only three of five specimens tested at 10°C (50°F) experienced ductile tearing. Each of the specimens was loaded to failure and the CTOD was designated δ_u. Specimens tested at 10°C (50°F) exhibited approximately 0.10 to 0.20 mm (4 to 8 mils) of ductile tearing and specimens tested at 21°C (70°F) exhibited approximately 0.26 to 0.41 mm (10 to 16 mils) of ductile tearing as shown in Figure 12. The extent of crack extension at both temperatures was insufficient to obtain a valid R-curve. The minor temperature difference (10°C to 21°C) was neglected and a linear regression performed on the combined six data points at 10°C (50°F) and 21°C (70°F) to obtain an estimate of δ_i. Ductile initiation of the deep crack specimen occurred at a CTOD value of 0.30 mm (12 mils).

The initiation of ductile tearing in the short crack specimen occurs at a CTOD level 1.5 times larger than the value for the deep crack specimen. This is consistent with the difference in short crack and deep crack specimen CTOD values at the first appearance of a ductile thumbnail. The difference in CTOD values for the short crack and the deep crack specimens at ductile initiation is not the same as at brittle initiation, δ_c, since the brittle-to-ductile transition temperature also is affected by a/W ratio. The temperature of the brittle-to-ductile transition for the short crack specimen occurs at a temperature 20°C (36°F) lower than the transition temperature of the deep crack specimens.

6.3 Weibull Distribution

A statistical analysis was conducted on the CTOD values at failure for the short crack and deep crack specimens. A two parameter Weibull distribution characterizes both the lower bound fracture toughness and the scatter in the lower shelf and lower transition regions. The Weibull distribution frequently is adopted to describe the critical event of brittle fracture [18–21] in support of the "weakest link" theory [21–23]. Appendix A provides the details of the two parameter Weibull distribution. The specimens are analyzed for testing temperatures at which brittle fracture represents the critical event; specimens with ductile tearing are treated as suspended tests. Table 4 summarizes results of the statistical analysis.

Figure 13 illustrates the Weibull analysis for the short crack and the deep crack specimens tested at -43°C (45°F). One of the nine short crack specimens has a small ductile thumbnail and is treated as a suspended test in the distribution. All eight of the deep crack specimens failed by brittle fracture and are included in the Weibull distribution. The short crack and the deep crack specimens have similar Weibull slopes of 3.36 and 3.61 respectively, indicating the same relative scatter. The 50, 90, and 95 percent probability values of the short crack specimens are, respectively, 2.63, 2.53, and 2.50 times larger than the probability values of the deep crack specimen. The arithmetic mean of CTOD values for the short crack specimens is 2.49 times larger than the mean for the deep crack specimens.

Figure 14 shows the Weibull analysis for the short crack and the deep crack specimens tested at -76°C (-105°F). The short crack specimens have a greater scatter in CTOD values reflected by a decrease in the Weibull slope. The short crack specimens have 50, 90 and 95 percent probability values of 2.59, 2.09, and 1.93 times larger than probability values for the deep crack specimen. The arithmetic mean of CTOD values for the short crack

specimens is 2.61 times larger than the mean for the deep crack specimens. The low coefficient of correlation for the short crack specimen (0.919) suggests the desirability of additional tests.

7. Discussion

The influence of crack–depth to specimen–width ratio (a/W) on fracture toughness values increases with the extent of plasticity developed in the specimen. In the lower–shelf region, the region of plastic deformation at the crack tip is extremely small with respect to the other specimen dimensions and is fully confined by unyielded material. To obtain valid K_{Ic} results (i.e., ASTM E–399), the radius of the plastic zone cannot exceed 1/50 of the specimen height, crack depth, or remaining ligament. For this very limited amount of plasticity, the lower–shelf fracture toughness is characterized by a single parameter (critical stress intensity factor) and is independent of specimen size, geometry, and crack depth.

In the lower–transition region, the increase of ductility allows the plastic zone to grow beyond the immediate crack–tip vicinity. Considerably more crack–tip blunting and larger plastic zones are present at fracture in the short crack specimens than in the deep crack specimens. Plastic zones extend to the free (tension) surface of the short crack specimens. Critical CTOD values for the short crack specimens (a/W = 0.15) are consistently 2.5 times larger than critical values for the deep crack specimens (a/W = 0.50).

Similar observations on the relative size of plastic zones are predicted by the *3–D* finite–element analyses of the short crack and deep crack specimens. Figure 15 illustrates the extent of plastic deformation corresponding to CTOD values of 0.067 mm (2.6 mils) and 0.028 mm (1.1 mils) which are, respectively, the critical CTOD values of the short and deep crack specimens tested at –76°C (–105°F). At the CTOD of 0.028 mm (1.1 mils), a plastic hinge has not yet formed in either specimen, yet the deep crack specimen fails at this level of deformation. To fail the short crack specimen at the same temperature, the CTOD must be increased to 0.067 mm (2.6 mils) with a much greater extent of plastic deformation as Fig. 15 illustrates (plastic hinge formation and yielding to the free surface behind the crack tip). However, the finite–element analyses reveal that equivalent opening mode stresses (on the crack–plane) are developed ahead of the crack tip in the short crack specimen at a CTOD of 0.067 mm (2.6 mils) and in the deep crack specimen at a CTOD of 0.028 mm (1.1 mils). Thus, although the specimen strains (and extent of plastic deformation) are markedly different at the two CTOD values, the important opening mode stresses ahead of the crack tip are the same.

Plastic zones for the short and deep crack specimens at CTOD values of 0.251 mm (9.9 mils) and 0.102 mm (4.0 mils) are shown in Figure 16. These correspond, respectively, to critical CTOD values for the short and deep crack specimens tested at –18°C (0°F). As in the previous comparison, equivalent opening mode stresses are developed ahead of the crack tip for the short crack specimen at a CTOD of 0.251 mm (9.9 mils) and the deep crack specimen at a CTOD of 0.102 mm (4.0 mils), even though the extent of plastic deformation is markedly different.

The increased plasticity observed in the experimental and finite-element analyses reduces "constraint" (stress triaxiality) along the crack front of the short crack specimen. A triaxial stress state ahead of the crack tip is necessary for the opening mode stress to increase above the simple uniaxial value given by the material stress-strain curve. When stress gradients and uncontained yielding no longer maintain the stress triaxiality, the elevated opening mode stress at the crack tip is partially relieved. Thus, to develop equivalent opening mode stresses ahead of the crack tip, the short crack specimen must undergo considerably greater deformation than the deep crack specimen to compensate for the reduced constraint. Larger strains imply increased crack-tip blunting and larger CTOD values. Al-Ani and Hancock [24] have demonstrated, through *2-D* finite-element analyses, a definitive loss of the HRR field [25,26] for short crack specimens as the plastic zone extends toward the free (tension) surface. The loss of HRR dominance is reflected by reduced opening mode stresses but increased near-tip strains as the global deformation disrupts the small-scale yielding fields characterized by the HRR solution. Consequently, a single, geometry (and load-level) independent fracture parameter (CTOD, *J*) does not appear to apply for the short crack specimens except for severely limited levels of plastic deformation. The Al-Ani and Hancock finite-element analyses are consistent with the *3-D* analyses of the present study; both confirm the experimental observations reported here.

Various investigators [13, 27, 28] have used the model proposed by Ritchie, Knott, and Rice [29], denoted RKR, to describe the effects of constraint on cleavage fracture. In the RKR model, cleavage fracture occurs when the maximum principal stress ahead of a sharp crack tip exceeds a critical value (σ_f) over a distance characterized by micro-structural effects. When a loss of constraint occurs, the triaxial stress state is relaxed, the opening mode stress ahead of the crack tip is relieved, and brittle fracture is delayed until the critical opening mode stress is achieved at greater deformation levels. Qualitatively, the RKR model confirms the significantly larger CTOD values for the short crack specimens in the lower-transition region where brittle fracture occurs following a loss of constraint caused by yielding to the free (tension) surface of the specimen.

The micro-mechanics of ductile crack initiation has been examined by numerous investigators including Ebrahimi [9], Ebrahimi, Matlock, and Krauss [30], and Green and Knott [31]. Ductile fracture initiates by tearing of microcracks and voids ahead of the blunted crack tip. Strain localizes in the ligaments between the microcracks and the blunted fatigue crack, causing the microcracks to grow and coalesce. If the *stress* intensification at the tip of the ductile microcrack reaches the critical fracture stress, cleavage fracture is triggered. However, the short crack specimens develop significantly greater CTOD levels (larger strains ahead of the crack tip) than the deep crack specimens at identical crack-tip stress levels. Consequently, ductile tearing initiates in the short crack specimens at a lower temperature than in the deep crack specimens, i.e., the critical *strain* for ductile tearing is developed before the critical stress required for cleavage fracture. Therefore the transition from brittle to ductile initiation in the short crack specimen occurs at a lower temperature than the transition in the deep crack specimen.

8. Summary and Conclusions

Laboratory tests were conducted on a low-strength structural steel (A36) to determine the effect of crack depth on the elastic-plastic, fracture toughness of square, three-point bend specimens. Fracture toughness was characterized by the crack tip opening displacement (CTOD). Short crack specimens having dimensions 31.8 * 31.8 * 127 mm (1.25 * 1.25 * 5.0 in.) with crack-depth to specimen-width ratios (a/W) of 0.15 were tested throughout the lower-shelf and lower-transition regions in which there is no stable crack growth prior to a brittle failure. Fracture toughness values for the short crack specimens were compared to experimental results for deep crack specimens, a/W = 0.50, having the same dimensions. The deep crack specimens were previously tested by Sorem et. al. [11]. Three-dimensional, finite-element analyses were employed to correlate experimentally measured quantities, load and CMOD, with CTOD values and plastic zone sizes at failure.

The results of this study support the following observations and conclusions:

1. In the lower-shelf region, where ASTM E-399 requirements on plastic deformation are satisfied, the short and deep crack specimens have the same critical CTOD values. The three-dimensional finite-element analyses for the two specimens reveal that the opening mode stresses ahead of the crack tip are identical at the same (critical) CTOD levels. These two observations confirm the independence of fracture toughness values on crack depth when the failure mode is stress controlled cleavage with severely limited crack-tip plasticity.

2. At identical temperatures within the lower-transition region, the short crack specimens have critical CTOD values approximately 2.5 times larger than values for the deep crack specimens. The *3-D* finite-element analyses reveal equivalent opening mode stresses ahead of the crack tip in the two specimens when compared at their respective, critical CTOD values. The extent of plastic deformation at failure in the two specimens is markedly different even though stresses ahead of the crack tip are identical. In the short crack specimens, plasticity spreads to the free (tension) side behind the crack tip and forms a plastic hinge at failure, while plasticity remains confined to the crack tip at failure for the deep crack specimens. The large difference in crack-tip stress fields at identical CTOD levels, and consequently geometry dependent critical values, demonstrates the inability of single-parameter fracture mechanics (as currently developed) to characterize the response.

3. The initiation of ductile tearing for the short crack specimens occurs at a CTOD level (δ_i) approximately 1.5 times larger than the initiation value for the deep crack specimens. The 1.5 ratio applies at both the first detectable appearance of ductile tearing (a "thumbnail") and when the ductile tearing reaches 0.20 mm (7.9 mils) of crack extension (proposed as the amount of crack extension for the CTOD testing standard in ASTM).

4. The brittle-to-ductile transition temperature is also influenced by the crack-depth to specimen-width (a/W) ratio. The transition temperature for the short

crack specimens occurs at approximately 20°C (36°F) less than the transition temperature for the deep crack specimens. Consequently, the relative difference in CTOD values for the short crack specimens and the deep crack specimens at ductile initiation, δ_i, is less than the 2.5 ratio found for brittle initiation, δ_c.

This study convincingly demonstrates the significant effect of crack–depth to specimen–width ratio (a/W) on elastic–plastic fracture toughness values (CTOD) for laboratory specimens. Short crack specimens have larger critical CTOD values in the lower–transition region and at the initiation of ductile tearing. Moreover, short crack specimens exhibit ductile behavior at a lower temperature than deep crack specimens. These observations have considerable implications for the application of CTOD test results to failure analyses and for development of testing/design specifications. For failure and fitness–for–service analyses, the crack depth selected for laboratory testing should reflect the flaw size and crack–tip "constraint" present in the structure. Such an approach should improve the correlations between laboratory specimen tests and structural behavior. That is, the automatic adoption of lower bound toughness values obtained using deep crack specimens may be unduly conservative and costly.

9. Acknowledgments

Support for two authors (WAS, STR) was provided by the Subcommittee on Failure Modes in Pressure Vessel Materials, Pressure Vessel Research Committee of the Welding Research Council and by the American Iron and Steel Institute. Support for RHD was provided by the Fatigue and Fracture Branch of the David Taylor Research Center.

10. REFERENCES

[1] Matsoukas, G., Cotterell, B. and Mai, Y.W., "Hydrostatic stress and crack opening displacement in three-point bend specimens with shallow cracks," *Journal of the Mechanics and Physics of Solids*, Vol. 34, No. 5, 1986, pp. 499–510.

[2] de Castro, P. M., Spurrier, J. and Hancock, P., "An experimental study of the crack length/specimen width (a/W) ratio dependence on the crack opening displacement (COD) test using small-scale specimens," *ASTM STP 677*, American Society for Testing and Materials, 1979, pp 486–497.

[3] Sumpter, J.D.G., "The effect of notch depth and orientation on the fracture toughness of multi-pass weldments," *International Journal of Pressure Vessel and Piping*, Vol. 10, 1982, pp 169–180.

[4] Cotterell, B., Li, Q.F., Zhang, D.Z. and Mai, Y.W., "On the effect of plastic constraint on ductile tearing in a structural steel," *Engineering Fracture Mechanics*, Vol. 21, No. 2, 1985, pp. 239–244.

[5] Li, Q.F., "A study about $J_{Ic}$and δ_i in three-point bend specimens with deep and shallow notches," *Engineering Fracture Mechanics*, Vol. 22, No. 1, 1985, pp. 9–15.

[6] Li, Q.F., Zhou, L. and Li, S. "The effect of a/W ratio on crack initiation values of COD and *J*-integral," *Engineering Fracture Mechanics*, Vol. 23, No. 5, 1986, pp. 925–928.

[7] Zhang, D.Z., and Wang, H. "On the effect of the ratio a/W on the values of δ_i and J_{Ic} in a structural steel," *Engineering Fracture Mechanics*, Vol. 26, No. 2, 1987, pp. 247–250.

[8] Anderson, T. L., McHenry, H.I. and Dawes, M.G. "Elastic-plastic fracture toughness tests with single-edge notched bend specimens," *ASTM STP 856*, American Society for Testing and Materials, 1985, pp. 210–229.

[9] Ebrahimi, F., "A study of crack initiation in the ductile-to-brittle transition region of a weld," *ASTM STP 945,* American Society for Testing and Materials, 1988, pp. 555–580.

[10] Sorem, W.A., Dodds, R.H., and Rolfe, S.T. "An analytical comparison of short crack and deep crack CTOD fracture specimens of an A36 steel," to appear in *ASTM STP* for the 21st national symposium on fracture mechanics.

[11] Sorem, W. A., Dodds, R.H., and Rolfe, S.T. "An analytical and experimental comparison of rectangular and square crack tip opening displacement fracture specimens of an A36 steel," to appear in *ASTM STP 995*, American Society for Testing and Materials.

[12] Shoemaker, A.K. and Seeley, R.R., "Summary report of round robin testing by ASTM Task Group E24.01.06 on rapid loading plane-strain fracture toughness K_{Ic} testing," *Journal of Testing and Evaluation*, Vol. 11, No. 4, 1983, pp. 261–272.

[13] Dodds, R.H., and Lopez, L.A., "A generalized software system for nonlinear analysis," *International Journal for Advances in Engineering Software*, Vol. 2 No. 4, 1980.

[14] Dodds, R.H., and Lopez, L.A., "Software virtual machines for development of finite-element systems," *International Journal for Engineering with Computers*, Vol. 13, 1985, pp. 18–26.

[15] Dawes, M.G., "Elastic–plastic fracture toughness based on the COD and *J*–contour integral concepts," *ASTM STP 668,* American Society for Testing and Materials, 1979, pp. 307–333.

[16] Matsoukas, G., Cotterell, B. and Mai, Y.W., "On the plastic rotation constant used in standard COD Tests," *International Journal of Fracture*, Vol. 26, No. 2, pp. R49–R53.

[17] Dodds, R.H., "Plastic rotation factors for shallow crack bend bars," presented to ASTM Task Group E24.08.02 (Computational Techniques and Procedures), November 8, 1988, Atlanta, GA.

[18] Wallin, K., "The scatter in K_{Ic} results," *Engineering Fracture Mechanics*, Vol. 19, No. 6, 1984, pp. 1085–1093.

[19] Anderson, T.L. and Williams, S., "Assessing the dominant mechanism for size effects in the brittle–to–ductile transition region," *ASTM STP 905*, American Society for Testing and Materials, 1986, pp. 715–740.

[20] Rosenfield, A.R., and Shetty, D.K., "Lower–bound fracture toughness of a reactor–pressure–vessel steel," *Engineering Fracture Mechanics*, Vol. 14, No. 4, 1981, pp. 833–842.

[21] Landes, J.D. and Shaffer, D.H., "Statistical characterization of fracture in the transition region," *ASTM STP 700,* American Society for Testing and Materials, 1980, pp. 368–382.

[22] Logsdon, W.A., "Elastic plastic (J_{Id}) fracture toughness values: their experimental determination and comparison with conventional linear–elastic (K_I) fracture toughness values for five materials," *ASTM STP 590,* American Society for Testing and Materials, 1976, pp. 43–60.

[23] Logsdon, W.A. and Begley, J.A., "Dynamic fracture toughness of A533 Grade A Class 2 base plate and weldments," *ASTM STP 631,* American Society for Testing and Materials, 1977, pp. 477–492.

[24] Al–Ani, A. and Hancock, J.W., "*J*–dominance of short cracks in bending and tension," to appear in *Proceedings*, 7 th International Conference for Fracture, March, 1989, Houston, TX.

[25] Rice, J.R. and Rosengren, G.F., "Plane strain deformation near a crack tip in a power law hardening material," *Journal of the Mechanics and Physics of Solids,* Vol. 16, 1968, pp 1–12.

[26] Hutchinson, J.W. "Singular behavior at the end of a tensile crack in a hardening material," *Journal of the Mechanics and Physics of Solids,* Vol. 16, 1968, pp 13–31.

[27] Milne, I. and Chell, G.C., "Effect of size on the *J* fracture criterion," *ASTM STP 668,* American Society for Testing and Materials, 1979, pp. 358–377.

[28] Pisarski, H.G., "Influence of thickness on critical crack opening displacement (COD) and *J* values,"*International Journal of Fracture*, Vol. 17, No. 4, 1981, pp. 427–440.

[29] Ritchie, R.O., Knott, J.F., and Rice, J.R., "On the relationship between critical tensile stress and fracture toughness in mild steel," *Journal of the Mechanics and Physics of Solids,* Vol. 21, 1973, pp 395–410.

[30] Ebrahmi, F., Matlock, D.K., and Krauss, G., "On ductile crack initiation in notched bend specimens," *Scripta Metallurgica*, Vol. 16, No. 8, 1982, pp 987–992.

[31] Green, G. and Knott, J.F., "The initiation and propagation of ductile fracture in low strength steels," *Journal of Engineering Materials and Technology,* Vol. 98, Series H, No. 1, 1976, pp. 37–46.

[32] Weibull, W., "A statistical distribution function of wide applicability," *Journal of Applied Mechanics,* Vol. 18, 1951, pp 293–297.

Appendix A – Weibull Analysis

Applicability of the Weibull distribution [32] has been demonstrated for a wide variety of statistical problems. The Weibull model may be applied to physical phenomenon for which the occurrence of an event in any part of an object occurs in the object as a whole. Examples include determining the weakest link in a chain, the size effect on failures in solids, and the fatigue life of structures. Various investigators have utilized the Weibull distribution to describe the lower bound fracture toughness and to characterize scatter attributable to specimen size [18–21].

Results of the experimental CTOD tests were statistically modeled using the two parameter Weibull distribution:

$$P(x) = 1 - e^{-(x/\theta)^m} \tag{A-1}$$

where:

P(x) = probability that a given specimen has a value less than x
x = measured variable (CTOD)
θ = scale parameter associated with failure probability of 0.632
m = shape parameter (the Weibull slope)

On rearranging terms, the above expression may be written in the form:

$$\ln[\ln(\frac{1}{1-P(x)})] = m\ \ln(x) - m\ \ln(\theta) \tag{A-2}$$

where:

$$-m\ \ln(\theta) = \text{the intercept at x} = 1.0 \tag{A-3}$$

Linear regression was conducted on the experimental CTOD values to compute the Weibull slope and intercept. The median rank was determined for each specimen using the relation:

$$P(x) = 1 - (2)^{-\frac{1}{N}} + (\frac{n-1}{N-1})(2^{(1-\frac{1}{N})} - 1) \text{ for } N < 20 \tag{A-4}$$

where:

N = total number of samples
n = rank–order number
1–P(x) = probability that a given specimen had a value greater than (x)

Wallin [18] describes the assumptions of Weibull theory and the manner in which deviations in experimental conditions affect the observed scatter. First, the Weibull theory assumes a constant slope (m) and thus a random distribution of flaws is required for the scatter to be realistically modeled. The Weibull slope indicates the relative scatter of the fracture toughness values. The smaller the scatter, the greater the Weibull slope; similar

Weibull slopes imply similar absolute degrees of scatter. That is given an equal number of specimens for each set and equivalent Weibull slopes, if the lowest value obtained from one set of specimens is 2.5 times the lowest value obtained from the other set of specimens, the largest value obtained from the first set will also be 2.5 times the largest value of the second set.

Second, ductile tearing prior to brittle failure affects the effective volume of material (flaws) sampled and therefore may invalidate the Weibull assumptions. Specimens exhibiting stable crack extension are treated as suspended tests. That is, they serve to adjust the relative placement of the other data values, but the actual CTOD values for the suspended tests are not plotted.

Third, the experimentally determined values for the scatter are dependent on the number of tests conducted in determining the scatter. The coefficient of correlation reflects the applicability of the Weibull distribution to describe the test results. If the coefficient is low, additional tests may be required to more accurately define the distribution.

TABLE 1

CHEMICAL ANALYSIS, %

Steel	C	Mn	P	S	Si
A36	0.20	1.11	0.007	0.023	0.029

TABLE 2

MECHANICAL PROPERTIES

Steel	Yield Strength @ 0.2% offset	Tensile Strength	Elongation in 50.8 mm	Reduction in Area
A36	248 MPa (36 ksi)	460 MPa (66.8 ksi)	38%	67%

TABLE 3

YIELD STRENGTH ADJUSTED TO TEMPERATURE

Steel	Temperature (°C)	Yield Strength (MPa)	(ksi)
A36	21 to 0	248	36
	-18	262	38
	-43	290	42
	-76	345	50
	-112	462	67
	-195	793	115

TABLE 4

WEIBULL DISTRIBUTION STATISTICS

*(31.8 * 31.8 mm specimens)*

a/W ratio	Temp. °C (°F)	Slope	Coefficient of Correlation	Mean mm (mils)	Probability Values 50% mm (mils)	90% mm (mils)	95% mm (mils)
0.50	−18 (0)	6.71	0.978	0.166 (6.53)	0.168 (6.61)	0.127 (5.00)	0.114 (4.48)
0.15	−43 (−45)	3.36	0.952	0.233 (9.17)	0.249 (9.80)	0.142 (5.59)	0.115 (4.53)
0.50	−43 (−45)	3.61	0.952	0.0937 (3.69)	0.0945 (3.72)	0.0561 (2.21)	0.0460 (1.
81)							
0.15	−76 (−105)	3.58	0.919	0.0889 (3.50)	0.0894 (3.52)	0.0528 (2.08)	0.0432 (1.70)
0.50	−76 (−105)	6.06	0.940	0.0341 (1.34)	0.0345 (1.36)	0.0253 (0.996)	0.0224 (0.881)
0.15	−107 (−160)	4.28	0.999	0.0437 (1.72)	0.0439 (1.73)	0.0283 (1.11)	0.0239 (0.941)
0.50	−112 (−170)	5.67	0.963	0.0144 (0.567)	0.0145 (0.570)	0.0104 (0.409)	0.0092 (0.362)
0.15	−195 (−320)	9.48	0.987	0.0034 (0.135)	0.0035 (0.137)	0.0028 (0.112)	0.0026 (0.104)
0.50	−195 (−320)	10.99	0.950	0.0023 (0.092)	0.0023 (0.092)	0.0020 (0.079)	0.0019 (0.075)

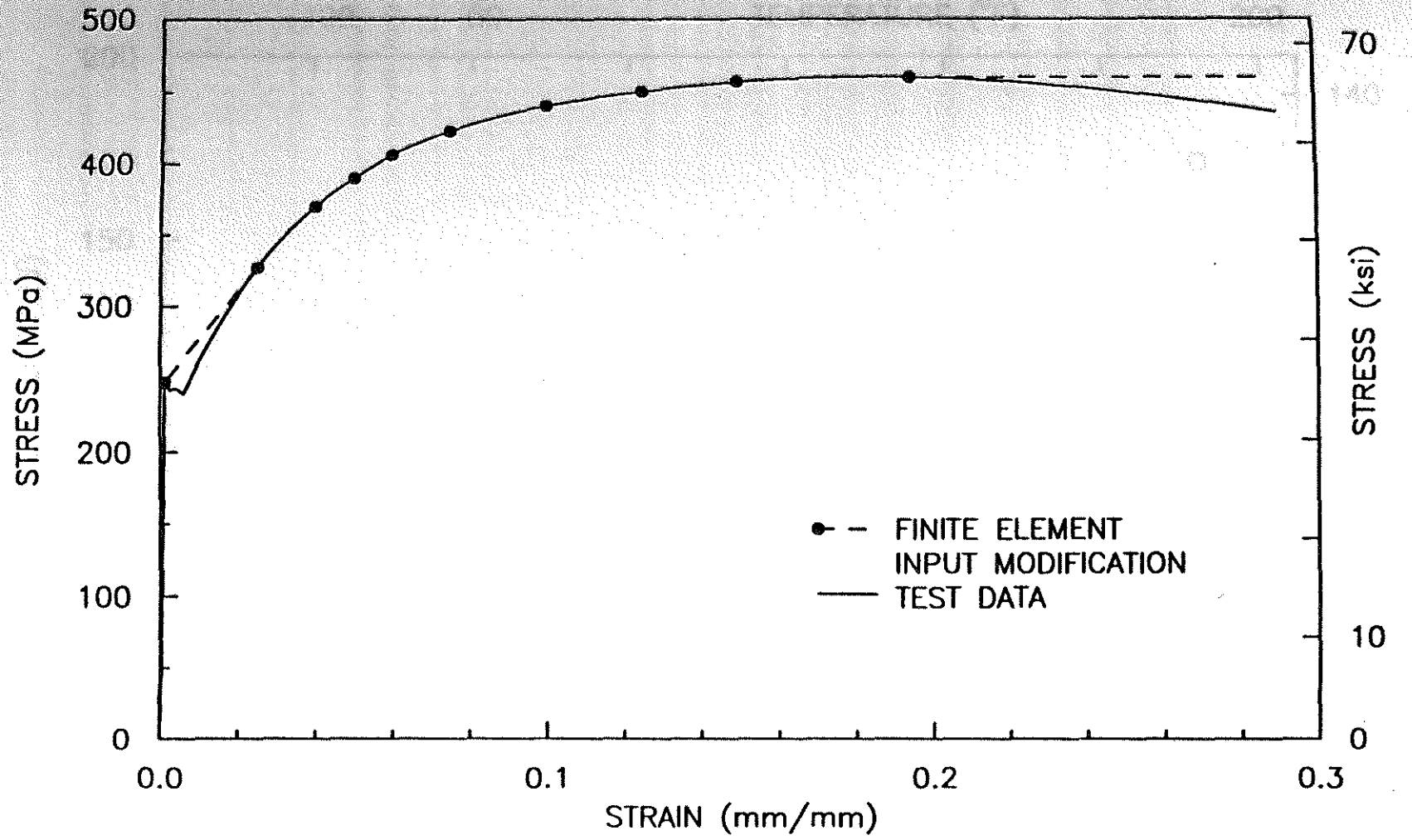

Fig. 1. A36 steel tensile stress–strain curve with modification for finite-element analysis.

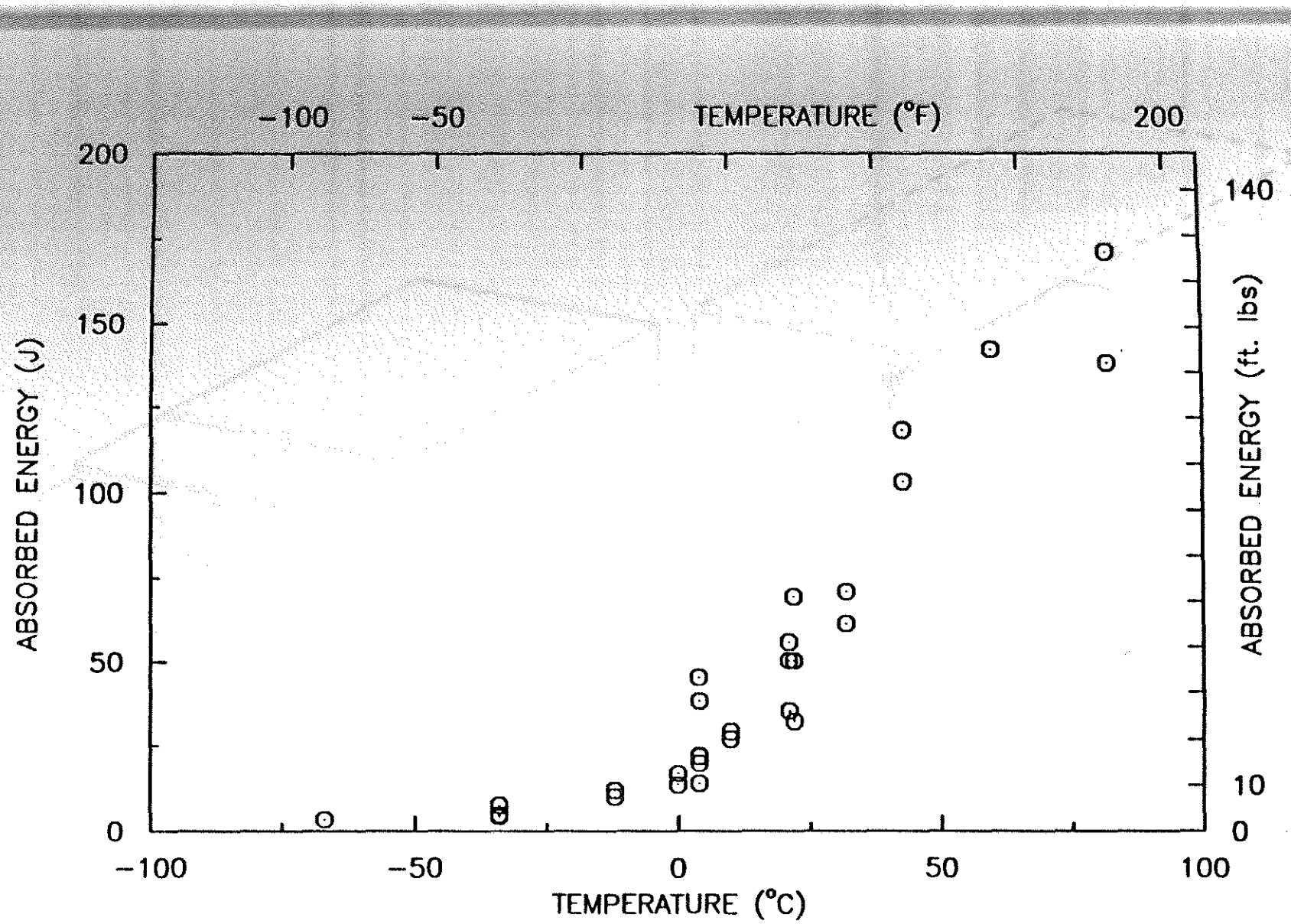

Fig. 2. CVN impact results for the A36 steel studied.

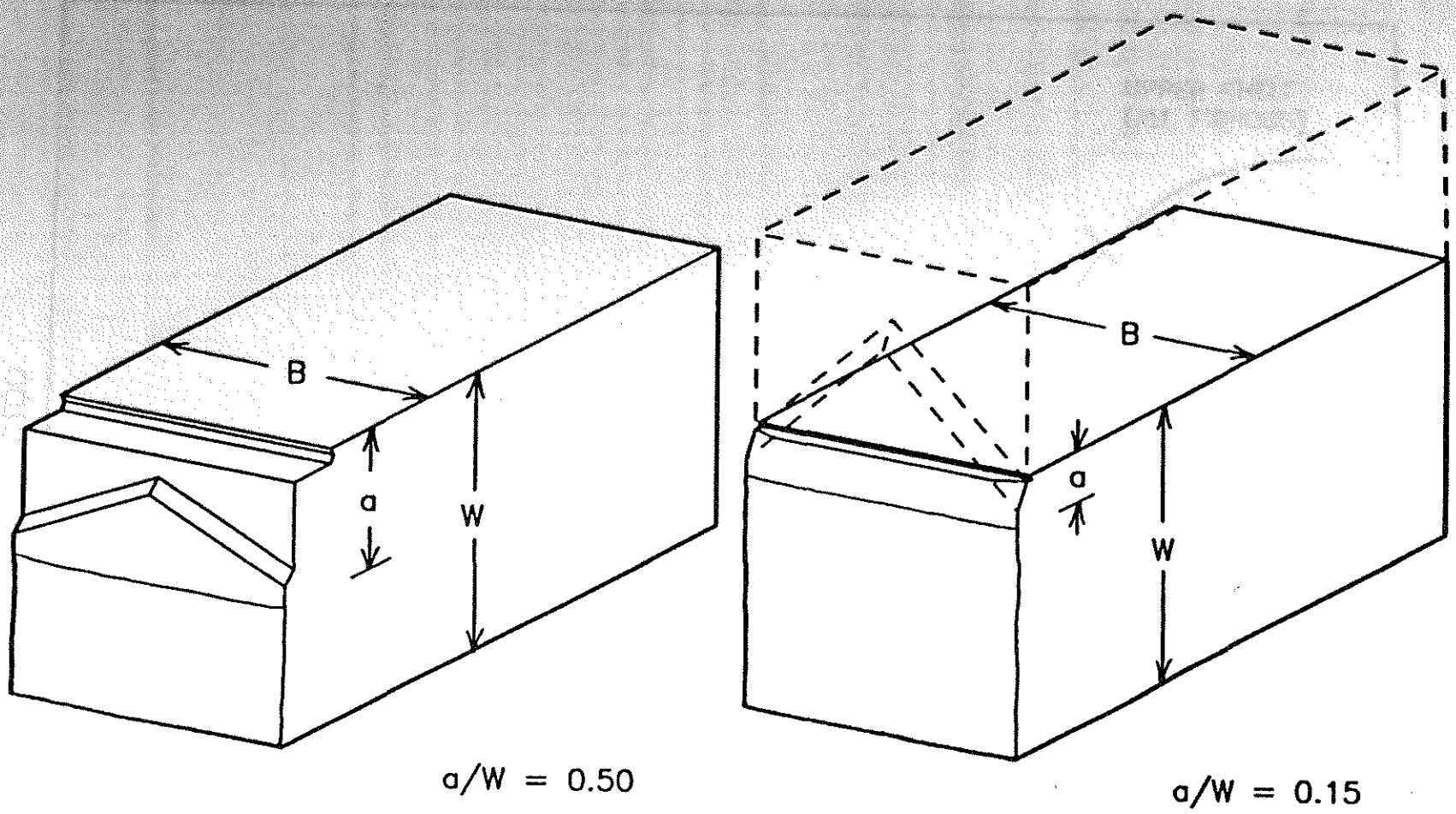

Fig. 3. Square cross–section (31.8 * 31.8 * 127 mm) three–point–bend test specimens.

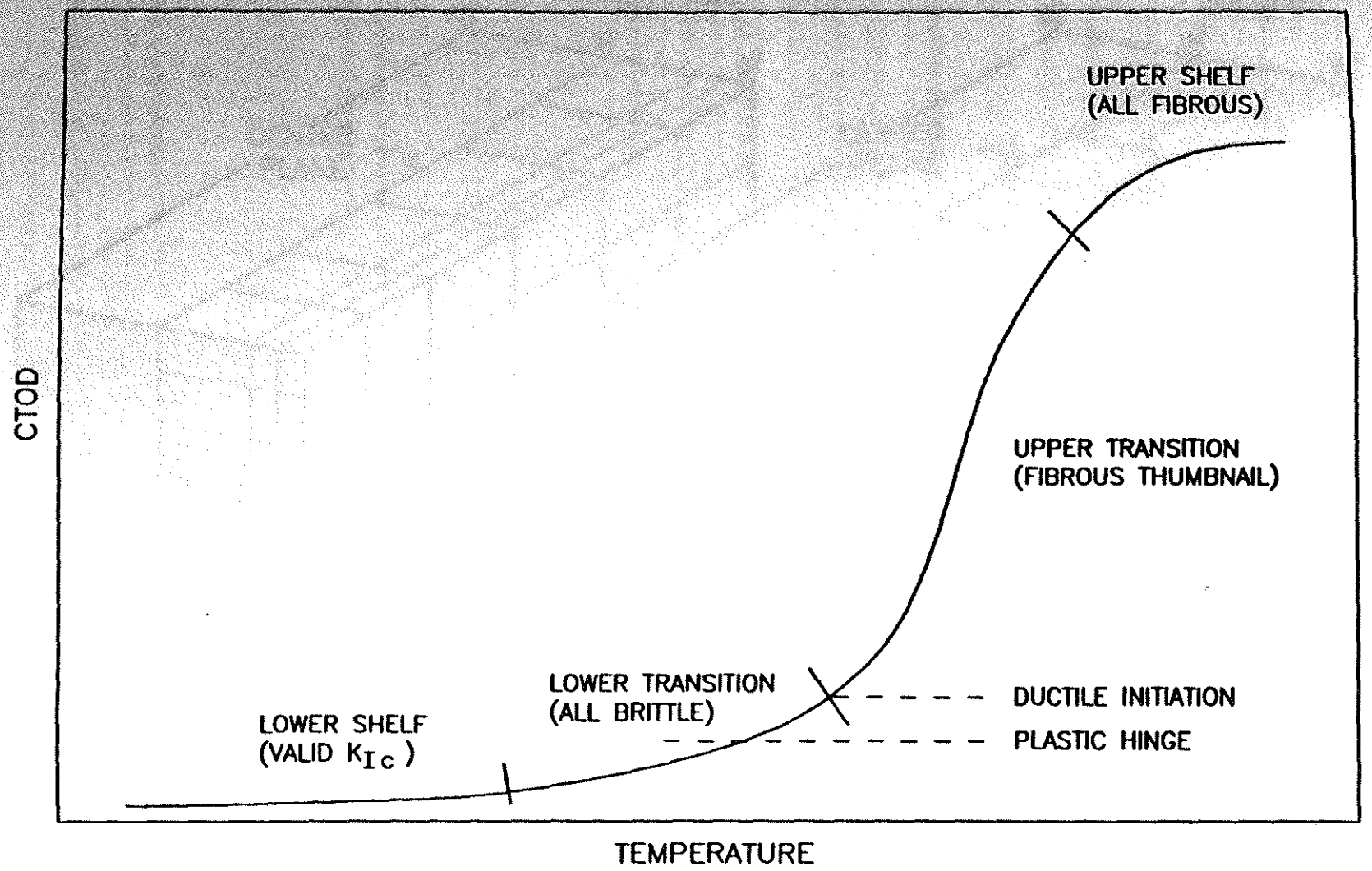

Fig. 4. Schematic CTOD–temperature transition curve.

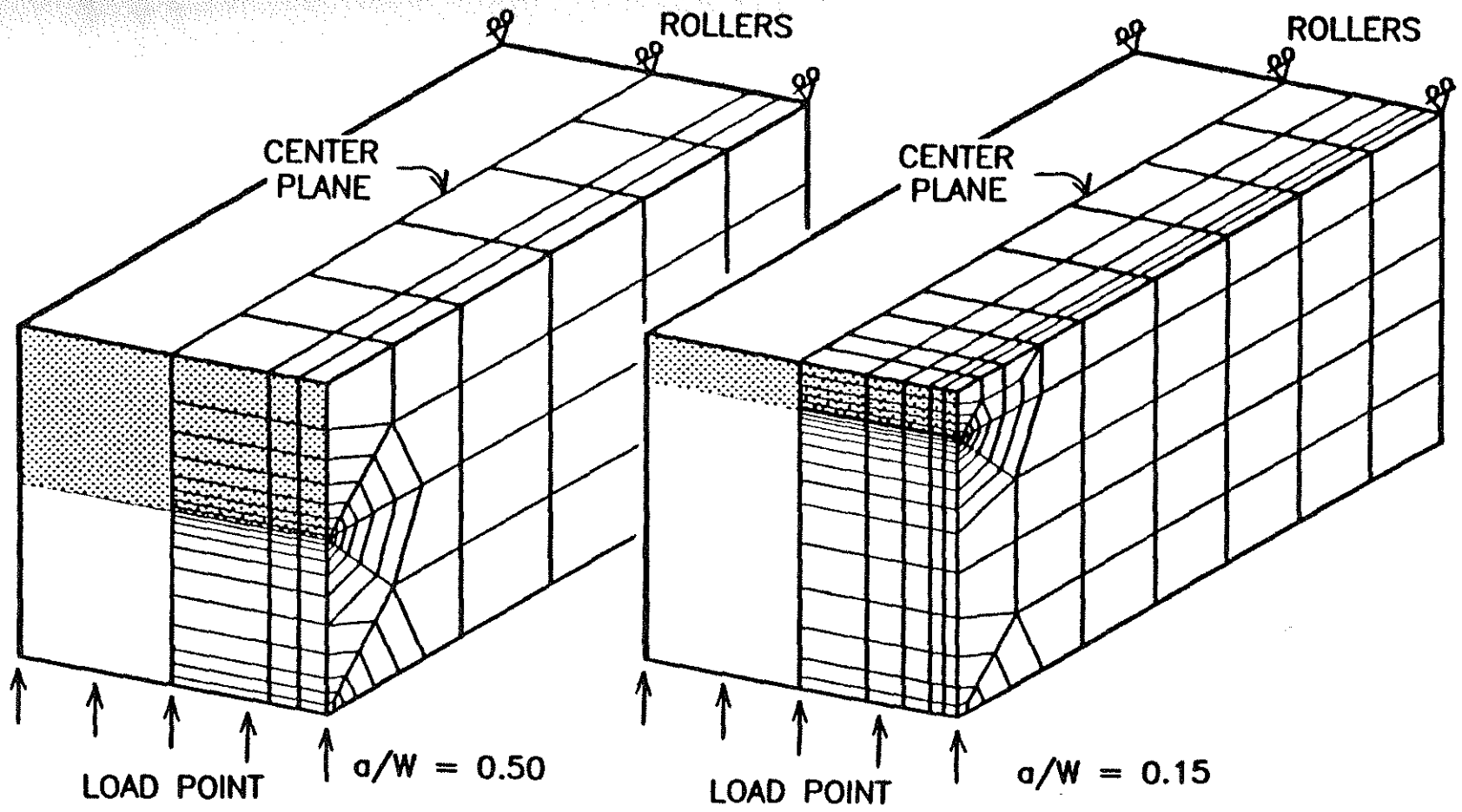

Fig. 5. Three-dimensional finite-element models for the bend specimens.

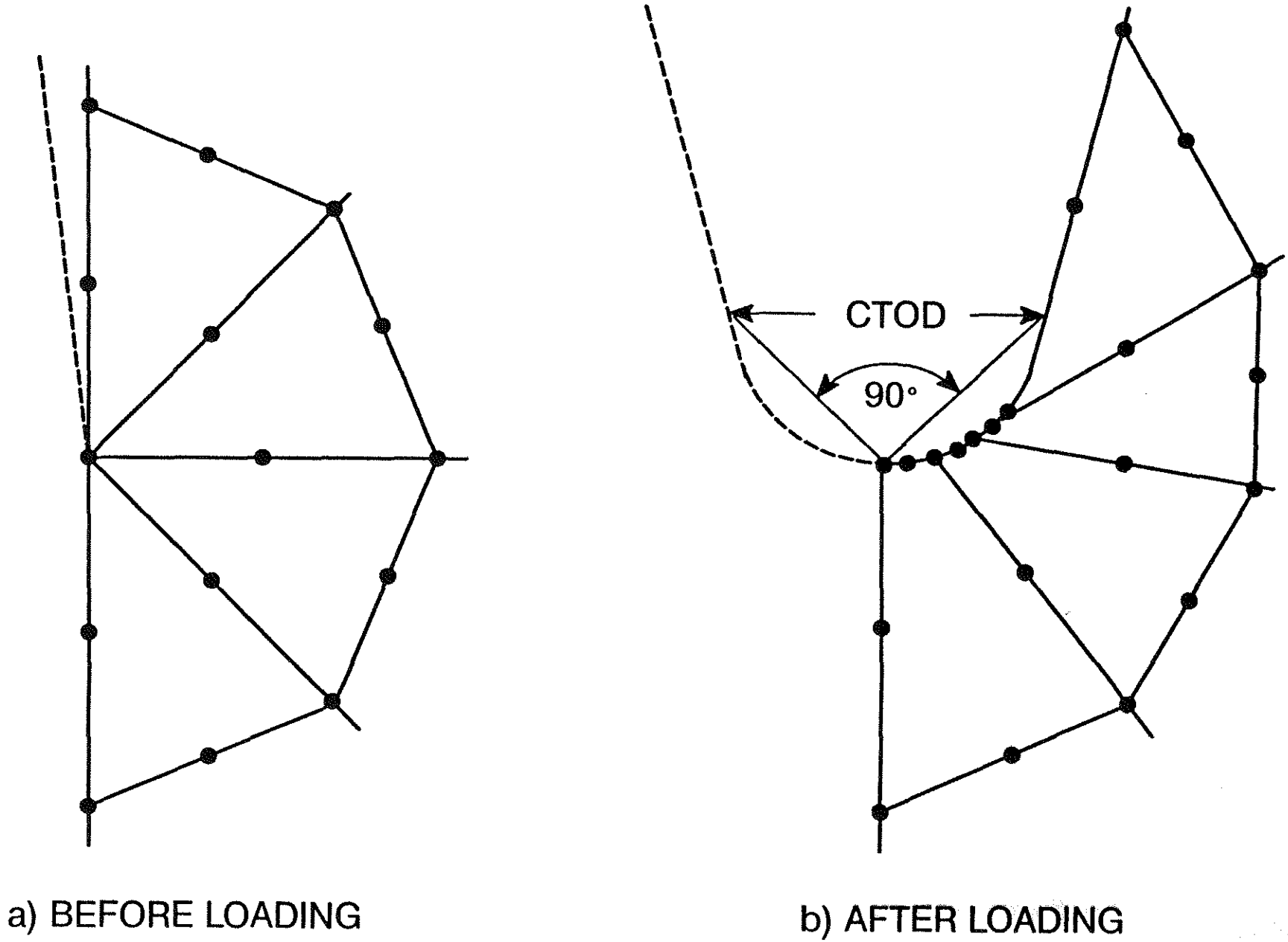

Fig. 6. 90° intercept procedure to define CTOD for finite-element analyses.

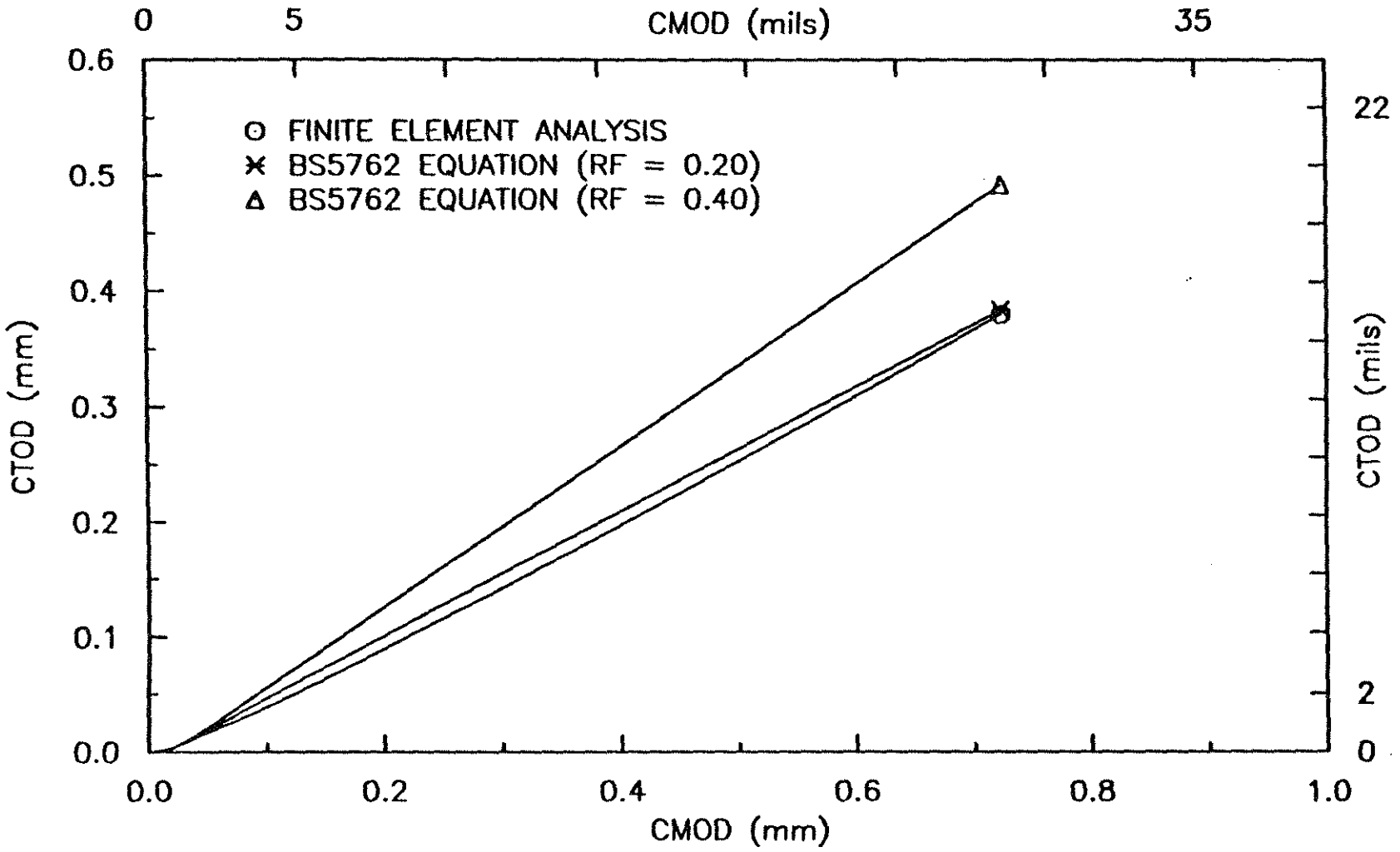

Fig. 7. CTOD vs. CMOD for square (31.8 * 31.8 mm) A36 steel specimens with a/W = 0.15.

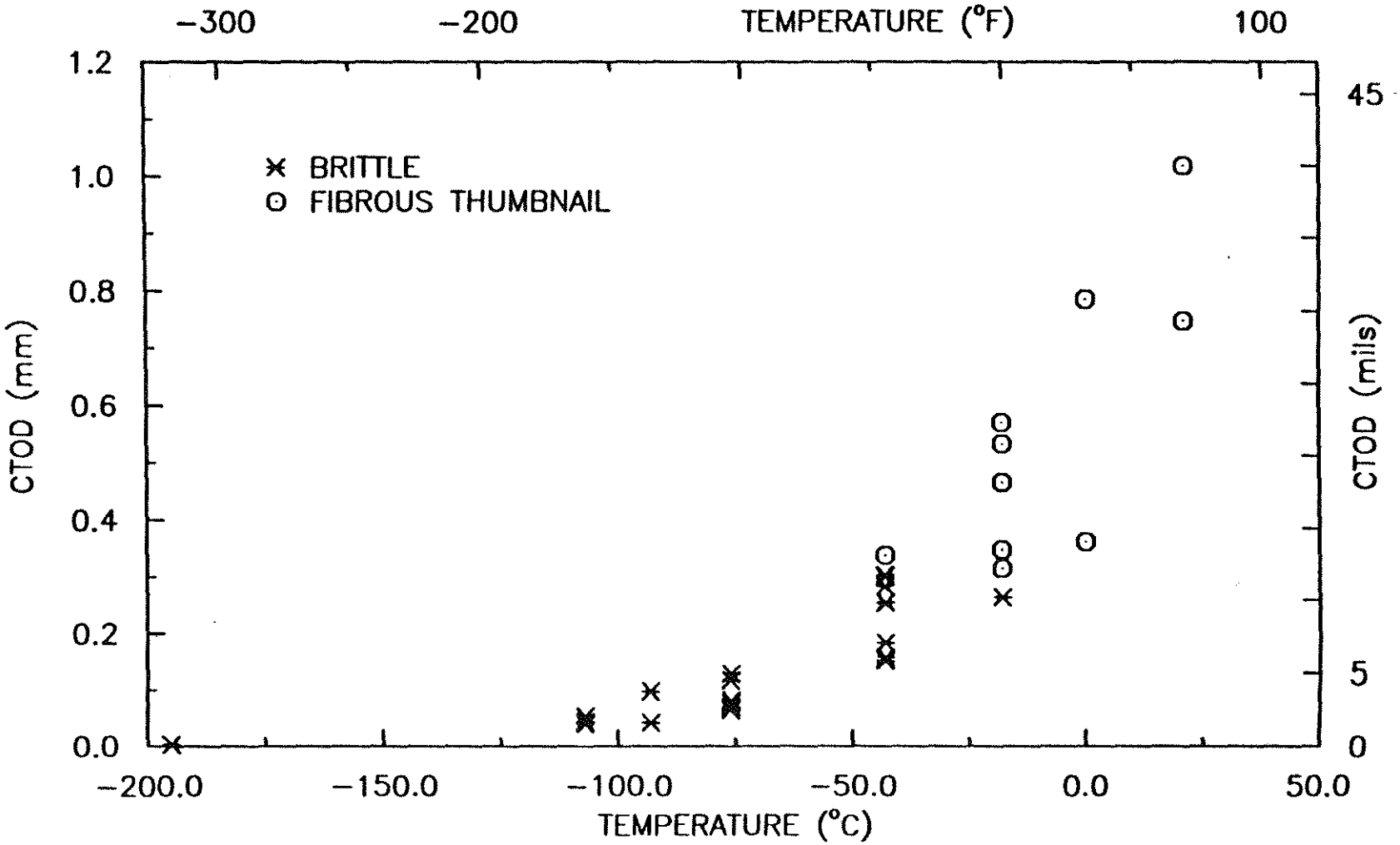

Fig. 8. CTOD vs. temperature for A36 steel specimens (31.8 * 31.8 mm) with a/W ratios of 0.15.

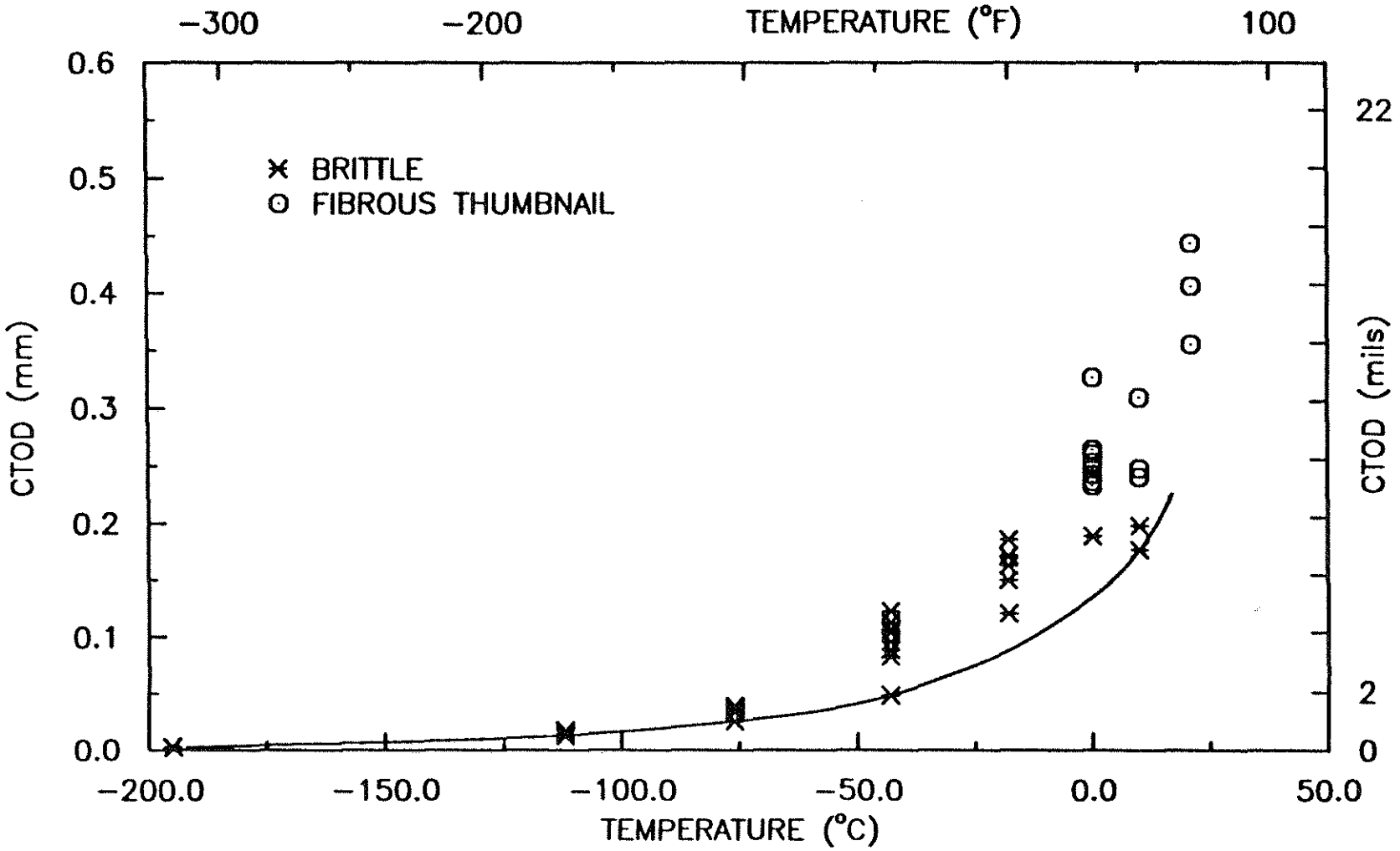

Fig. 9. CTOD vs. temperature for A36 steel specimens (31.8 * 31.8 mm) with a/W ratios of 0.50.

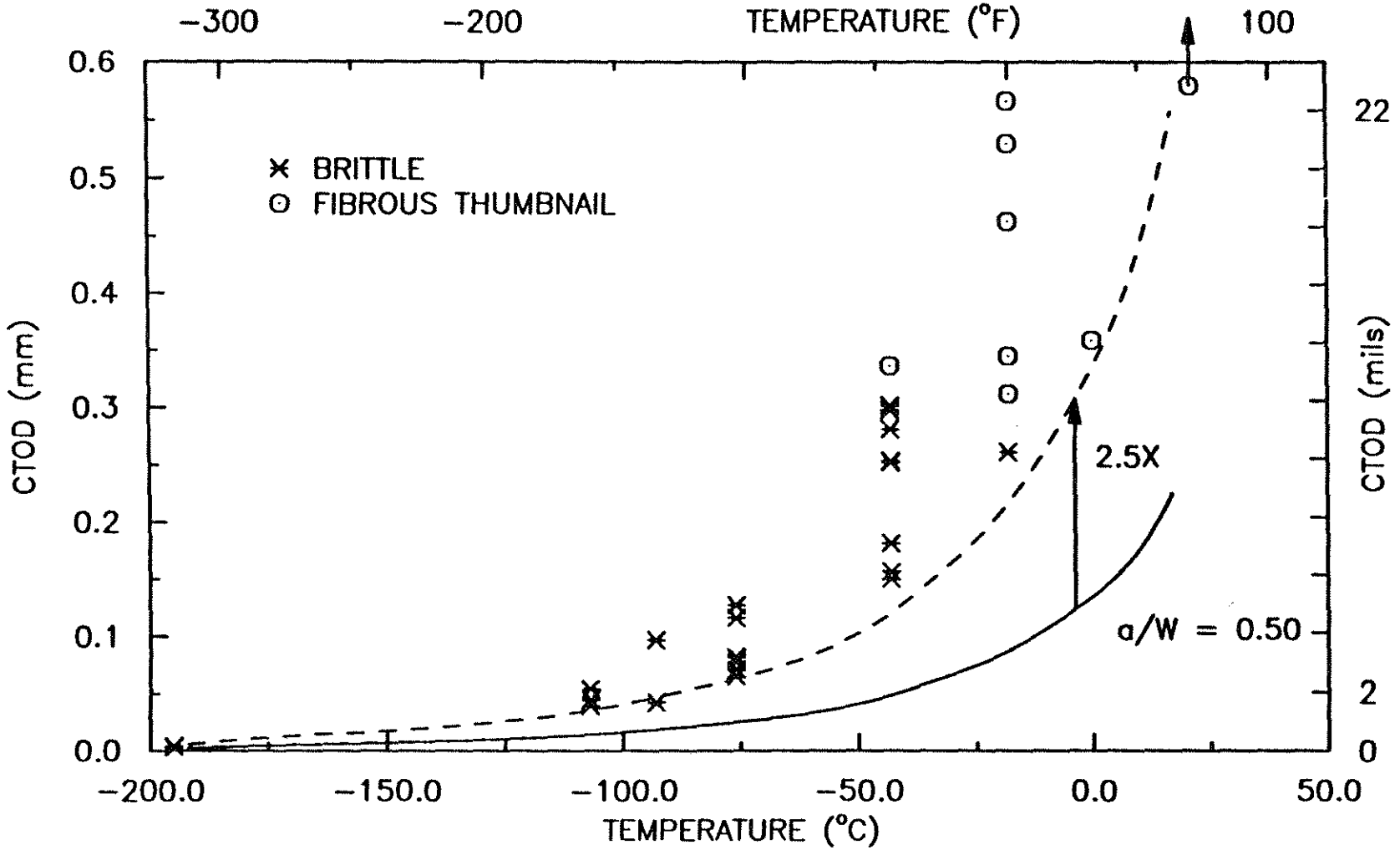

Fig. 10. Increase of critical CTOD values for shallow crack depth, A36 steel.

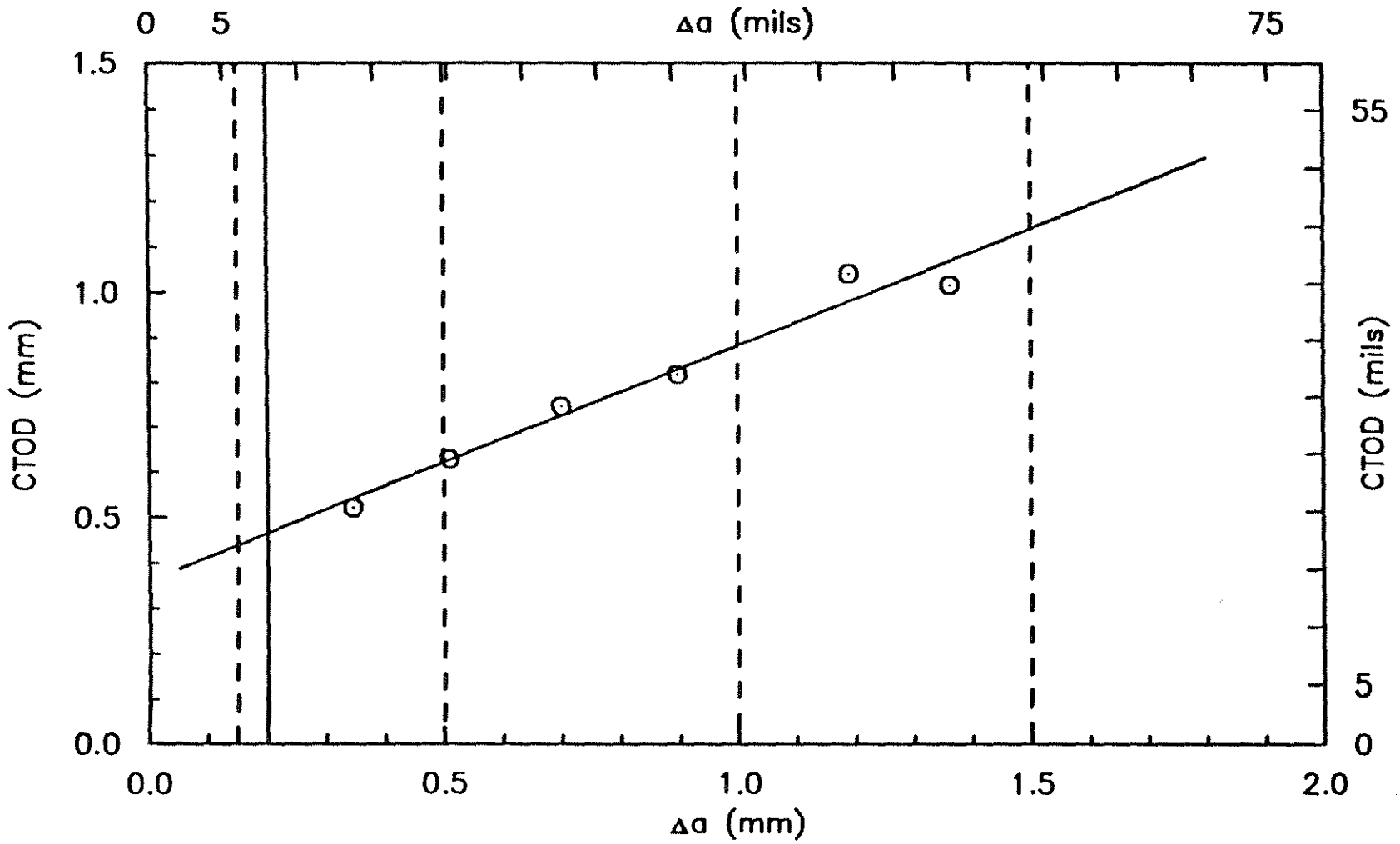

Fig. 11. CTOD vs. crack growth for A36 steel specimens (31.8 * 31.8 mm) with a/W = 0.15 at 21°C.

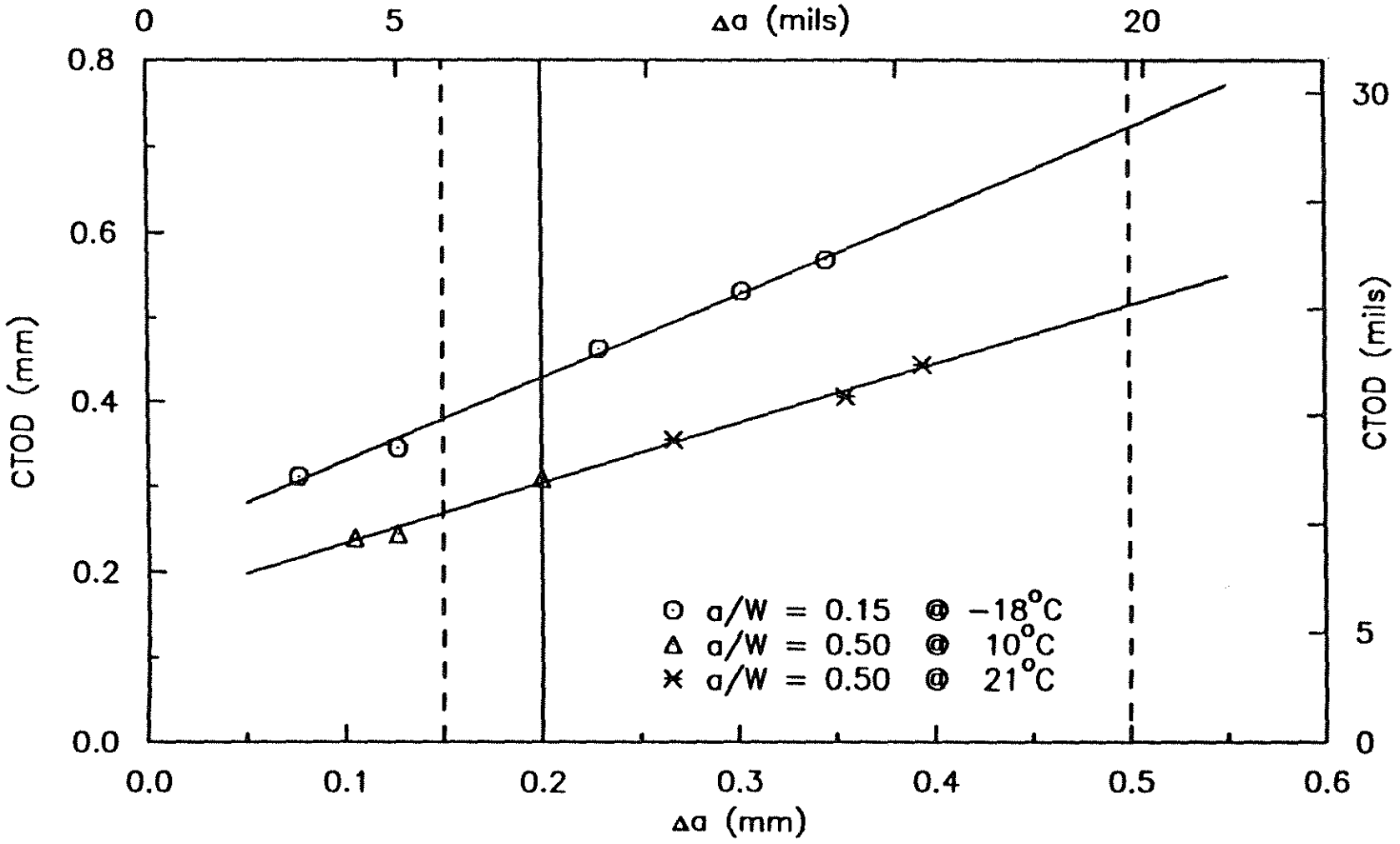

Fig. 12. Comparison of CTOD vs. crack growth for A36 steel specimens (31.8 * 31.8 mm) with a/W=0.15 and 0.50.

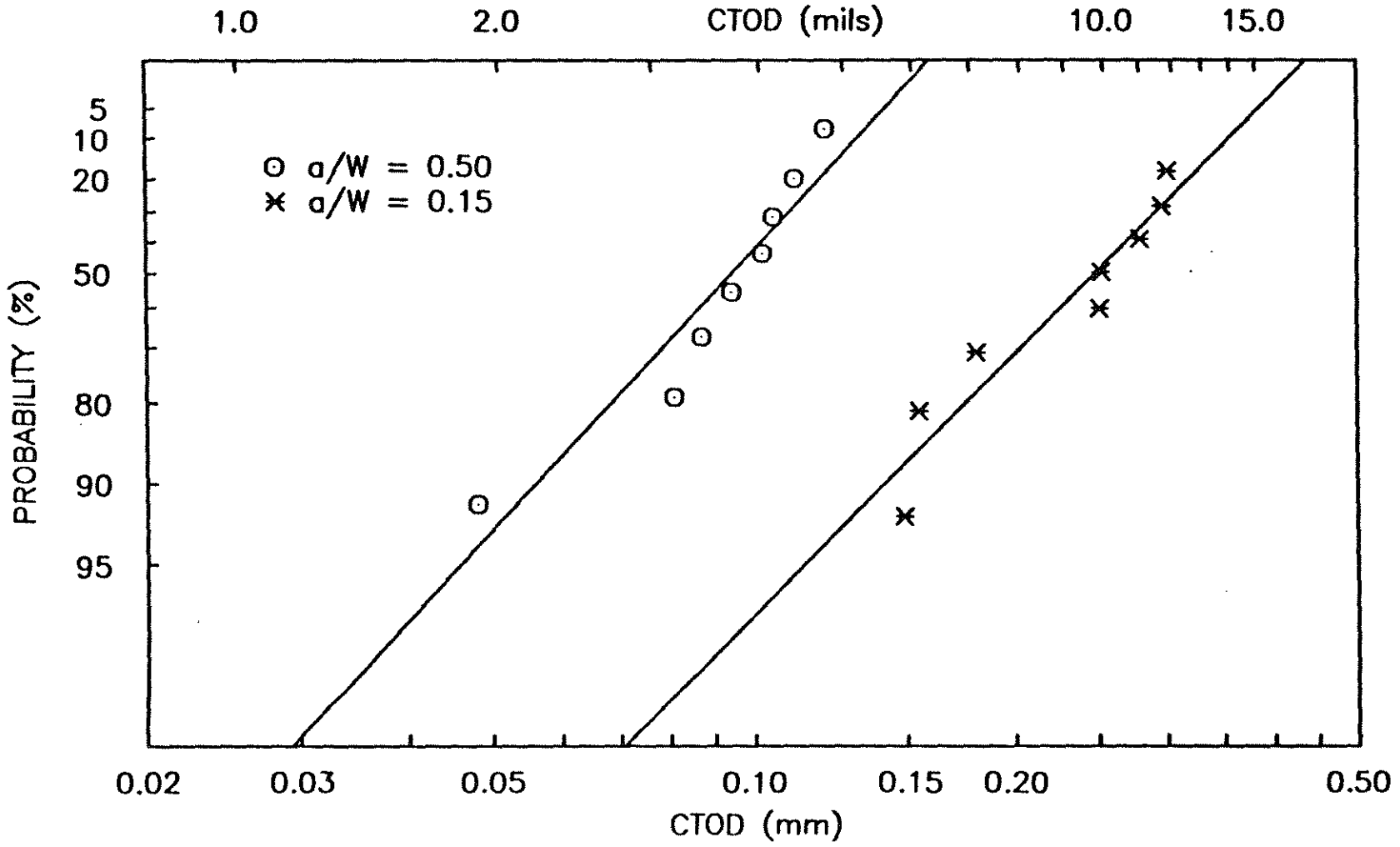

Fig. 13. Weibull distribution for the A36 steel specimens tested at −43°C (−45°F).

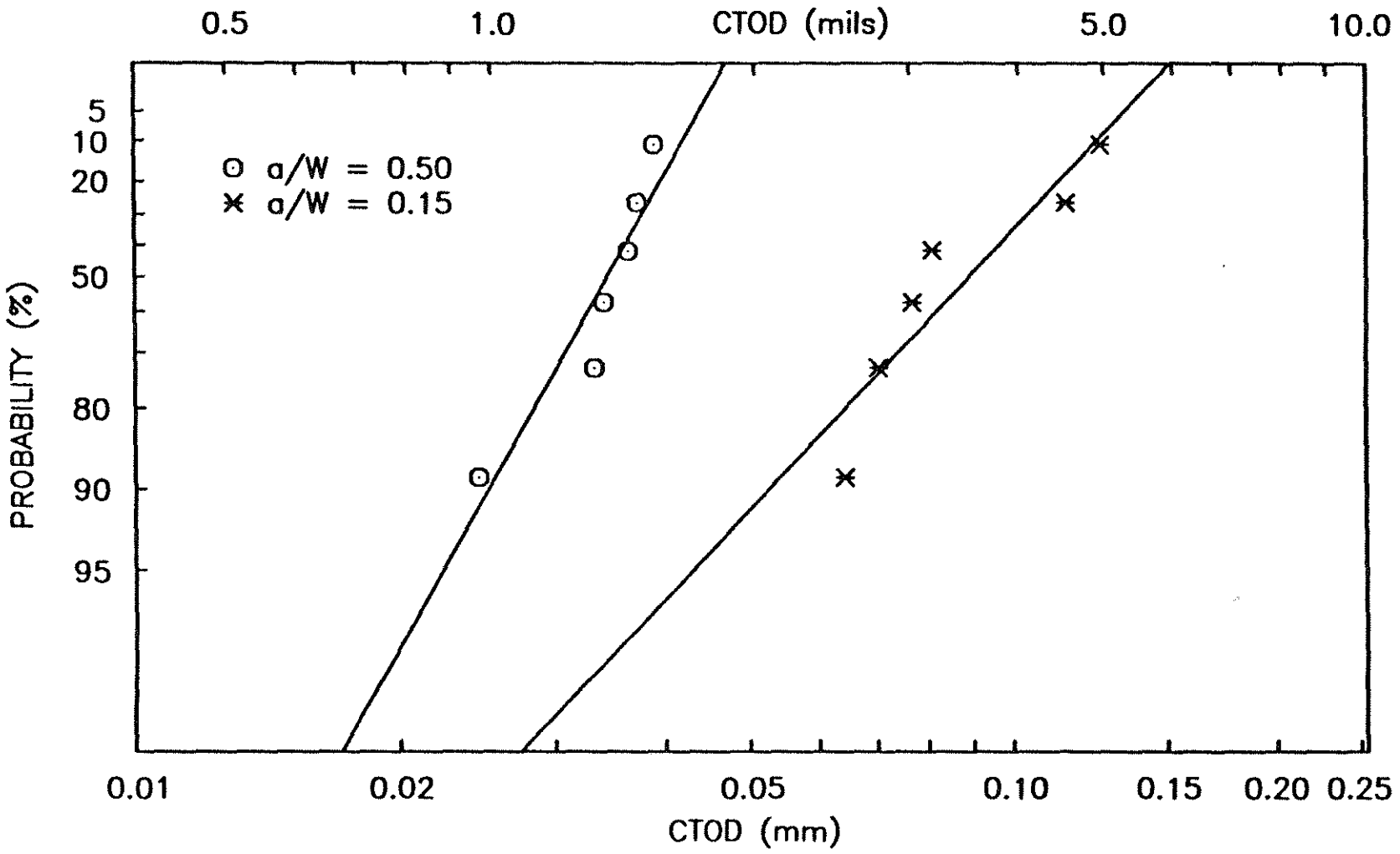

Fig. 14. Weibull distribution for the A36 steel specimens tested at –76°C (–105°F).

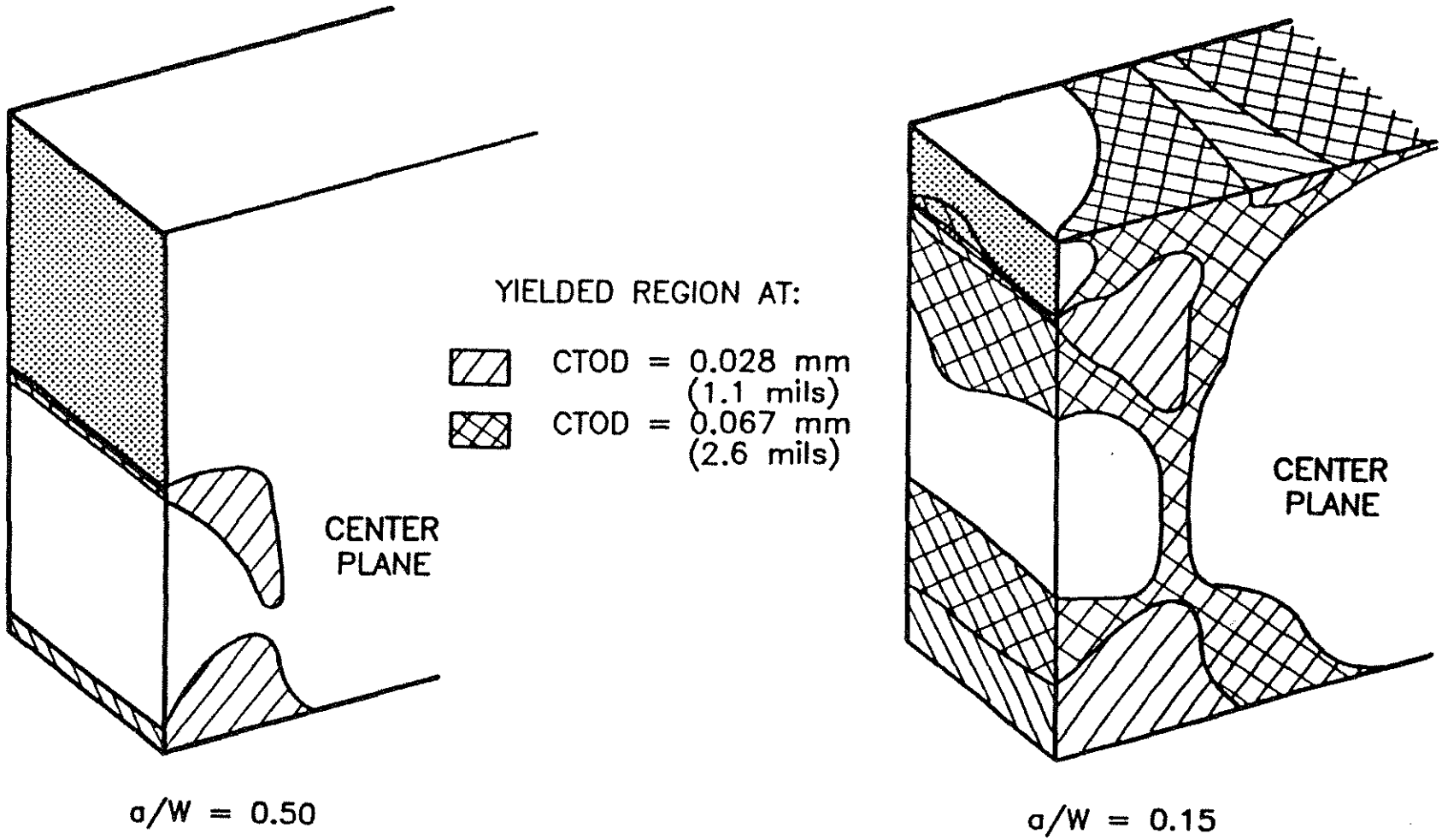

Fig. 15. Plastic zones for A36 steel specimens (31.8 * 31.8 mm) corresponding to critical CTOD values for specimens tested at –76°C (–105°F).

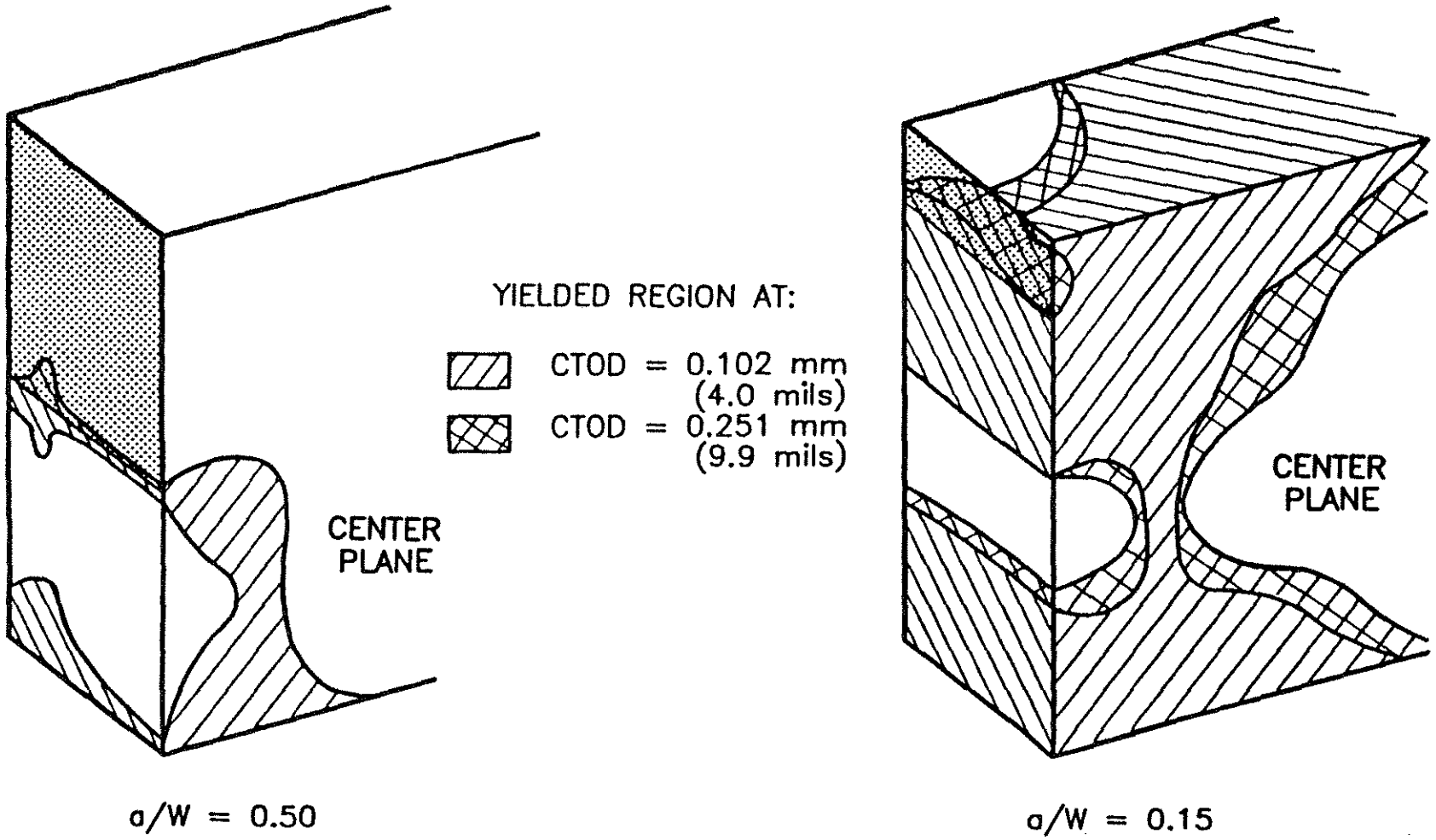

Fig. 16. Plastic zones for A36 steel specimens (31.8 * 31.8 mm) corresponding to critical CTOD values for specimens tested at –18°C (0°F).